Optimized Layout of Engineered Geothermal Systems and Potential in Germany

Master's Thesis

Charitra Jain

charitra.jain@rwth-aachen.de

Institute for Applied Geophysics and Geothermal Energy
E.ON Energy Research Center
RWTH Aachen

Supervisors:
Prof. Dr. Christoph Clauser
Dr. Darius Mottaghy

July 31, 2012

Acknowledgements

The last five months have been a great learning experience for me. This project would not have been possible without the help of a lot of people and I am highly indebted to them. Foremost, I would like to thank Prof. Christoph Clauser for being an amazing guide. To Christian Vogt, for being patient with me while I asked him all those numerous questions. To Darius, for his valuable input and to all the GGE members for providing me a comfortable environment to work in. To Carin, Cristina, Rahul and Roy for keeping me motivated and being there whenever I needed some advice. And to my family and friends for the continuous moral support and helping me maintain my focus throughout the project.

Abstract

Geothermal energy is environmentally friendly, renewable and ubiquitous and yet only a tiny fraction of it is harnessed commercially for heat and electricity generation. In the absence of natural steam reservoirs, Engineered Geothermal System (EGS) technologies can tap this energy source to supply year-round base load power, but the process of heat extraction from the subsurface needs optimization. Forward modelling code SHEMAT simulates EGS reservoirs by solving coupled partial differential equations governing fluid flow and heat transport. Building on EGS's strengths of inherent modularity and storage capability, it is possible to implement multiple wells in the reservoir to extend the rock volume accessible by circulating geothermal fluids for absorbing more heat. By varying parameters like production flow rates and well-locations in the subsurface, this study looks at their long-term impacts on the reservoir development. This approach allows us to experiment with different placements of the engineered fractures and propose several EGS layouts for achieving optimized heat mining. Considering the available crystalline area while accounting for the land cover under protected areas, seismically hazardous zones, and infrastructure; this study evaluates the overall EGS potential in Germany and its possible contribution towards national power production. Engineered Geothermal Systems make a compelling case for exploiting the heat stored in the Earth's crust in a future powered by a sustainable, decentralized energy system.

Contents

List of Figures

List of Tables

Chapter 1

Introduction

This chapter provides an introduction to geothermal energy, establishes its potential contribution towards global energy needs, and summarizes its applications based on the available heat production technologies. Chapter 2 introduces the EGS concepts, discusses its implementation and outlines the outstanding challenges that need to be addressed for ensuring an EGS project's success. Chapter 3 discusses the forward model required to simulate the fluid flow and heat transport, optimizes the model and proposes several EGS layouts for effective heat mining. Chapter 4 calculates the EGS potential in Germany and determines its contribution towards national power production.

1.1 Geothermal Energy

Geothermal energy is a renewable energy source that has a great potential to contribute significantly towards world's ever-increasing energy demands. It is the thermal heat stored in the solid earth and its internal fluids. Mankind has reaped the benefits of geothermal energy in the form of hot springs for centuries, but only in the last 100 years the technological advancements have made it feasible to tap this energy source effectively and use it for a variety of applications like space heating and electricity generation. An emphasis has been made recently on the development of geothermal exploitation techniques as geothermal energy has a limited CO_2 footprint and can help mitigate climate changes in cooperation with other renewables [3].

1.2 Geothermal Resources and Reservoirs

Earth provides us with copious amounts of thermal energy in the form of heat flow in the continental crust. Radioactive decay of uranium (^{235}U), thorium (^{232}Th) and potassium (^{40}K) at depths and the upward convection and conduction of heat from the earth's core and mantle are the two primary processes during this

heat flow. Magma intrusions result in local accentuation of the heat flow in the continental crust [39]. The accessible resource base i.e. the amount of heat that can be produced theoretically from the uppermost 5 km of earth's surface is in the order of 140,000,000 EJ. But a very small fraction of it (5000 EJ) falls under the accessible resource base, which is expected to become economical in the next 40 - 50 years. According to McKelvey's classification of resources [29], geothermal reserves i.e. the resources with high economic feasibility and low geological uncertainty only account for 0.00036 % (500 EJ) of the total accessible resource base [15].

The geothermal resources are classified in four groups depending on the environments in which they are found. Hydrothermal resources consist of high temperature (up to 350 °C) water or steam at moderate depths (1 km – 4 km) in permeable regions of porous rocks. Geopressured resources are overpressured brines with significant amounts of dissolved natural gas (CH_4) at very high temperatures found in deep sedimentary basins near offshore petroleum deposits. In case of Hot Dry Rock or Engineered Geothermal System resources, the reservoir needs stimulation for producing hot fluids. Magma resources consist of molten rock at very high temperatures of 700 °C – 1200 °C at an accessible depth ($<$ 7 km) [15].

The grade of all geothermal resources depends on the geothermal gradient dT/dz; with temperature T and depth z), reservoir rock permeability and porosity, and the amount of fluid saturation [39]. Several types of installations and technologies already exist to harness hydrothermal resources effectively. Groundwork has been done for exploiting the geopressured environments but it requires further research to make the process economical and efficient. For utilizing magma resources, materials need to be developed that can withstand extremely high temperatures and corrosive nature of magma [17]. Optimizing the heat extraction from Engineered Geothermal System reservoirs is an engineering issue and it will be dealt extensively in this master's thesis.

Geothermal fields are either water-dominated (low enthalpy warm water resource with temperatures less than 100 °C or medium enthalpy wet steam resource with temperatures lying between 100 °C – 150 °C) or vapor-dominated with high enthalpy dry steam as the resource and temperatures greater than 150 °C [15].

1.3 Advantages

Geothermal energy has many advantages when compared to other renewables (solar, wind, hydroelectric) and fossil fuels. To start with, it can be used over a wide spectrum of temperatures and volumes while other resources become economical only if they exceed a certain minimum size. Inherent storage capability

and independence from external factors like seasonal variations make geothermal energy suitable for year round electricity production and base load electric and thermal power supply [3]. It is environmentally benign with minor carbon footprint in general, and low toxic gas emissions (CO_2, H_2S, SO_2). The surface expression of geothermal plants is limited as no mining operation is required. A land area between $2\,km^2$ – $20\,km^2$ is enough to establish a well field that can support a 100 MW geothermal plant. The land can be simultaneously utilized for livestock grazing or fisheries. It is a common practice to re-inject the cooled brine or treated wastewater from local communities, for instance at The Geysers, USA [20] to support the reservoir pressure thus extending the life of a geothermal plant. This prevents contamination of shallow aquifers by chemical species like arsenic (As), boron (B), ammonia (NH_3) and mercury (Hg) present in the brine [26].

Geothermal energy is considered as a renewable source of energy as the heat stored in the earth gets replenished on a geological time scale. Undoubtedly, geothermal energy scores heavily in ecological and economical aspects when compared to fossil fuels and nuclear energy. It should be incorporated with other renewables to build the lower carbon-energy future.

1.4 Applications

Geothermal energy can be used directly for space heating, i.e. heating residential or official buildings and industrial applications. Alternatively, it can be used for electric power generation by converting thermal energy into electricity at some expense. Resources are exploited more efficiently when it comes to direct use, as all energy can be used unlike in the conversion from heat to electricity. Heat conduction and heat advection are the two main transport processes on which all technologies rely to extract thermal energy from the subsurface. Heating plants based on heat diffusion into an isolated underground heat exchange system avoid exchange of any substance or direct contact with the subsurface rock. Hot fluids or brines are produced from geothermal fields by heat advection and are utilized both for direct use and electric power generation [15].

1.4.1 Direct Use

A variety of diffusion-based earth-coupled heat extraction systems and heat advection based hydrothermal heating systems exist to provide heat for space heating and sometimes for cooling as well. Horizontal earth-coupled heat exchangers require a large surface area and consist of a heat exchange fluid circulating through an underground pipe system at about 2 m depth that collects heat by diffusion. Shallow borehole heat exchangers consist of one or several U-pipes (either at 90°angle or in coaxial configuration) installed in a borehole whose depth varies

between 50 m – 250 m. Heat is extracted by the primary circulation within these U-pipes and sent to secondary circuit. Heat exchanger piles are integrated directly into the concrete foundations of buildings. Deep borehole heat exchangers consist of an inner production pipe and outer borehole casing arranged coaxially reaching up to depths of about 1500 m – 3000 m and temperatures of about 60 °C – 110 °C (only in Germany). Hydrothermal heating system consists of several deep boreholes (injectors, producers) that produce large volumes of hot fluids from the deep reservoirs. The transport mechanism is highly influenced by underground reservoir rock's permeability and porosity, reservoir thickness and transmissivity $\boldsymbol{T}$ ($\boldsymbol{T} = K.d$; i.e. the product of hydraulic conductivity K and reservoir thickness d). Geothermal energy also has numerous industrial applications like pulp, paper and wood processing, hydrogen production, and metal galvanization [15].

1.4.2 Electric Power Generation

Even though direct use of geothermal heat from hot springs dates back to several millennia, electric power generation from geothermal energy started only a century ago in Lardarello, Italy, in the year 1904. Based on the reservoir parameters, different types of geothermal plants are required to harness the geothermal energy. In the presence of natural steam or hot water reservoirs, forcing high-pressure steam or organic vapor to drive the turbines generates electricity. Engineered Geothermal Systems are employed when neither natural steam nor hot water is available and reservoirs lack sufficient permeability for effective heat transfer [15].

Vapor-dominated reservoirs are easy to produce but are very scarce in number [20]. They are exploited by dry steam plants (Figure 1.1, middle) that pump hot steam through wells from the underground to turn the turbines for electricity generation. Used steam is either exhausted to the atmosphere (non-condensing plant) or condensed and recycled (condensing-plant) when non-condensable gases weigh less than 15 % of total steam. Such systems are modular with capacities ranging from 20 MW_e – 120 MW_e and have been operational, e.g., in Lardarello, Italy (543 MW_e), The Geysers, USA (888 MW_e) and Kamojang, Indonesia (140 MW_e).

Water-dominated wet steam reservoirs like boiling springs and geysers are more abundant than vapor-dominated ones. Pressurized water at high temperatures acts as a geothermal resource and is exploited by wet steam plants (Figure 1.1, left). To protect the turbine blades from corrosion, liquid water is evaporated into steam using multiple separators (flash systems) at the surface. Since the produced fluid contains a lot of dissolved minerals like chlorides, bicarbonates, silicates, etc. it is re-injected back into the reservoir. Flash steam power plants are under operation around the world, for example in Matsukawa, Japan

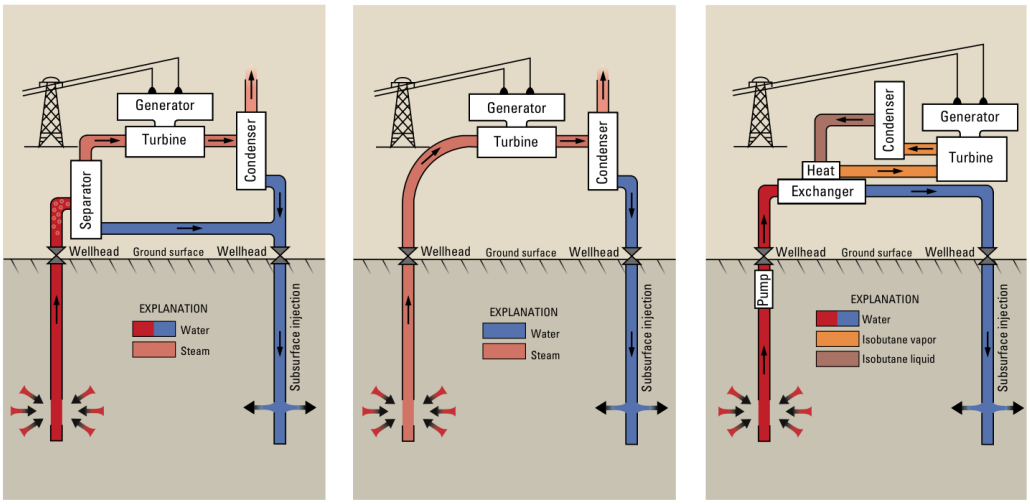

Figure 1.1: Electricity generation from water-dominated flash steam plant (left), vapor-dominated dry steam plant (middle) and moderate-temperature binary plant (right) [17].

(24 MW_e), Imperial Valley, USA (327 MW_e double flash) and Wairakei, New Zealand (327 MW_e triple flash).

Binary plants (Figure 1.1, right) are the most efficient ones when it comes to exploiting medium temperature resources (around 85 °C) from low enthalpy water-dominated hot water reservoirs that are present around the world at accessible depths. They are different from dry or wet steam plants in the sense that the brine is not in direct contact with the turbines or the atmosphere. The geothermal heat from the produced hot brine in primary loop evaporates a low boiling-point working fluid in secondary loop that drives the turbine generator. The Organic Rankine Cycle (ORC) uses halogenated hydrocarbons (Freon, Frigen), propane and isobutane whereas the Kalina cycle uses a mixture of ammonia (NH_3) and water as the working fluid. The Kalina cycle has improved exergy (fraction of energy that can be converted into other forms) efficiency by 10 % - 20 % over ORC owing to variable temperature range over which the ammonia-water mixture boils. Binary plants are operated, e.g., in Unterhaching, Germany (28 MW_t + 3.4 MW_e) and Landau, Germany (6 MW_t + 2.9 MW_e). Combined cycle plants running at Svartsengi, Iceland (45 MW_e), Puna, Hawaii (30 MW_e) and Leyte, Philippines (125 MW_e) have both flash system plants and ORC systems [15].

Only the technologies that harness thermal energy from natural steam or hot water reservoirs have been discussed so far. They have undergone extensive development over the years and by now have reached a well-established stage. These systems do not exist all around the world and are rather confined to regions like tectonic plate boundaries, mid-ocean ridges, subduction zones

and volcanoes. In the absence of natural steam reservoirs, one has to resort to Engineered Geothermal Systems (EGS) for electricity production. Unlike conventional geothermal resources, EGS resources are not limited in distribution and have enormous potential for recovering earth's thermal energy.

Chapter 2

Engineered Geothermal Systems

2.1 Defining EGS

The idea behind EGS is to emulate the permeability of a viable hydrothermal system by engineering the reservoir. It is a simple extrapolation of naturally occurring hydrothermal systems. Two or three wells are drilled into the subsurface reservoir reaching depths up to 5 km and terminating several hundred meters apart. Water is circulated from the injection to the production wells through a system of open, connected fractures where it gets heated by contact with the rocks.These systems are either open or form a closed loop as shown in Figure 2.1. The fracture network in the host rock is created by different stimulation technologies. EGS can be implemented anywhere as long as rock temperatures are high enough to support it. Reservoirs with insufficient hydraulic permeability are tackled with hydraulic fracturing. In principle, any accessible volume of hot dry rock can become an EGS reservoir provided that it is economical. EGS is inherently modular and theoretically scalable from $10^0\,\mathrm{MW}_e$ – $10^2\,\mathrm{MW}_e$.

Owing to its great potential towards meeting world energy needs, several research projects have been conducted around the world aiming at developing EGS methods. There are several issues that limit the productivity of an EGS reservoir and among them having insufficient connectivity between production and an injection well is the most prominent constraint. This thesis is studying the reservoir response towards stimulating the reservoir rock by creating different fractures and optimizing the layout of EGS reservoirs.

2.2 Subsurface Design Issues for EGS

Success or failure of every EGS project depends heavily on the understanding of the reservoir beforehand. Factors like geothermal gradient, rock porosity and

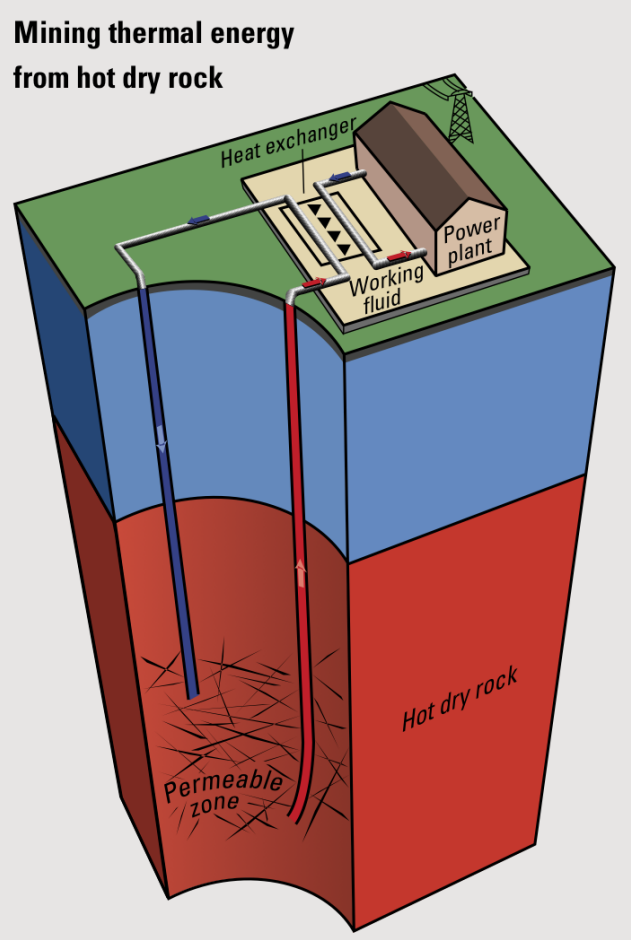

Figure 2.1: Simplified representation of EGS. Cold water (blue) is pumped down the injection well where it gets heated by the hydraulically fractured permeable rock and returns to the surface as hot produced water (red) from production well for electricity production [17].

permeability, reservoir geology with existing stress regimes, rock-fluid interactions and susceptibility to seismicity not only control the physical process of heat extraction, but also determine the economics of energy production [39].

The geothermal gradient allows us to estimate how much heat is in place and how efficient it would be to produce electricity. Natural permeability controls the pressure drop in the wells. It is necessary to know the geology of the reservoir including its faults, fractures and geodynamic history as they influence the mechanical and thermal properties of the rock and thus the results of the simulations. Knowledge of lithology is important before drilling as it affects the drill bit life, penetration rate, and drilling costs. Study of stress regimes gives us an insight about the orientation of tensile structures and state of stress along

faults. Hydraulic fracturing either enhances or creates permeability when none exists in Enhanced or Engineered Geothermal Systems respectively. Stresses on rock along with the reservoir rock's elastic properties determine the extent of these enhanced or newly created fractures and their resultant transmissivity [39]. Depending on the direction of these fractures, deviated wells are drilled cutting through them ensuring good hydraulic conductivity. The distance between wells is kept long enough to avoid short-circuiting and, at the same time, it has to be short enough to avoid an undesired pressure drop [42].

Rock-fluid interactions over a long time pose a great uncertainty for EGS feasibility. The circulated water gets cooled by the energy conversion system over years and does not remain in geochemical equilibrium with rock minerals. Permeability and connectivity of stimulated reservoir change with time owing to dissolution and precipitation of minerals. Problems of scaling are dealt by using scale inhibitors and brine acidification. There is still a need to better understand the long-term impacts of rock-fluid interactions on the economics and properties of EGS reservoir [39, 20, 26].

EGS projects in proximity to urban environments have received much public criticism and disapproval when it comes to induced seismicity. When water is injected under high pressures to stimulate the reservoir, it increases the pore pressures at depth, which reduces the effective strength of the subsurface rocks thus triggering the release of tectonic stress and causing tremors or even small earthquakes. Stimulation in geothermal reservoirs near geodynamically active regions has higher chances of inducing seismicity. The magnitude of induced seismicity depends at what rate the fluid is injected, how much slip occurs along the fault, how much stress already existed on the fault before slipping and how extensive the local fault system is. A correlation has been found between water injection and induced seismicity in terms of increased number of low magnitude seismic events. No damaging event has ever happened so far to the surrounding communities, but the Basel Deep Heat Mining Project in Switzerland [27] was shut down amid public concerns. Such unfortunate incidents can and should be avoided by employing proper drilling practices and carrying out a seismic risk investigation as part of the EGS feasibility study. It is speculative that operating an EGS reservoir for sustained periods can trigger a felt earthquake. It has been proposed that re-injection of waste fluids can thus also help in releasing enormous amounts of energy stored in earth's surface by triggering low-intensity events. This would mitigate chances of a major natural disaster that could result from instantaneous release of this stored energy. As the induced seismicity poses a threat to the society, an understanding needs to be established between the industry operators and the public through open communication. Moreover, induced seismicity can act as a viable reservoir management tool by monitoring its development over the years [27].

2.3 Reservoir Stimulation and EGS Implementation

Many hydrothermal system projects that were left undeveloped initially owing to insufficient permeability now have a chance to see the light of the day by reservoir stimulation techniques. Not only do these techniques include hydraulic fracturing to increase permeability, but they also deal with fault and fracture analysis and directional drilling of wells to intersect fractures with favorable orientation [17]. In order to create highly conductive fractures, different stimulation techniques exist. In hydraulic fracturing, highly pressured fluids are injected into the subsurface rocks via injection wells to create new fractures or enhance existing fractures for permeability [15]. These stimulations are either water fracs (i.e. those using water), gel-proppant fracs or a combination of both called hybrid fracs [42]. These proppants stay in the fractures to keep them open even when the hydraulic pressure is removed [38]. Critically stressed rocks fail, shear and produce fractures during stimulation. As the near-wellbore region experiences the highest pressure drop, hydraulic fracturing is the most effective there [39]. Direction of fracture opening and propagation depends on the existing stress regimes. When difference between maximum compressive stress (σ_1) and minimum compressive stress (σ_3) is small, fractures initiate in several directions. At high stress ratios ($\sigma_1 >> \sigma_3$), fractures propagate perpendicular to minimum compressive stress (σ_3) and accordingly well doublet is aligned along (σ_3). Fracture behavior in response to local stress regimes is shown in Figure 2.2. It is important to remember that fractures open in a direction parallel to the minimum compressive stress (σ_3) but propagate in the direction of maximum compressive stress (σ_1) [35].

Very high flow rates are required for an EGS project to be economically feasible. It is only possible when the reservoir transmissivity is high. At the same time, the residence-time of the fluid residing in pore spaces should be long enough so that it is heated up by the reservoir rock. Both goals of long residence-time and high transmissivity are accomplished by having a large number of complex fractures [39]. In addition to hydraulic stimulation, chemical stimulation (fracture and matrix acidizing) and explosive fracturing (controlled underground explosions) are also considered to create or enhance permeability but will not be discussed in detail [15].

2.4 Review of EGS Achievements

A number of EGS case studies have been undertaken around the world to demonstrate the feasibility of heat production from stimulated and engineered reservoirs. The HDR project at Fenton Hill, New Mexico was the pioneering work in the field of EGS [12]. Adapting techniques from hydrocarbon industry, several vertical 'penny-shaped' fractures were created in the reservoir with the minimum

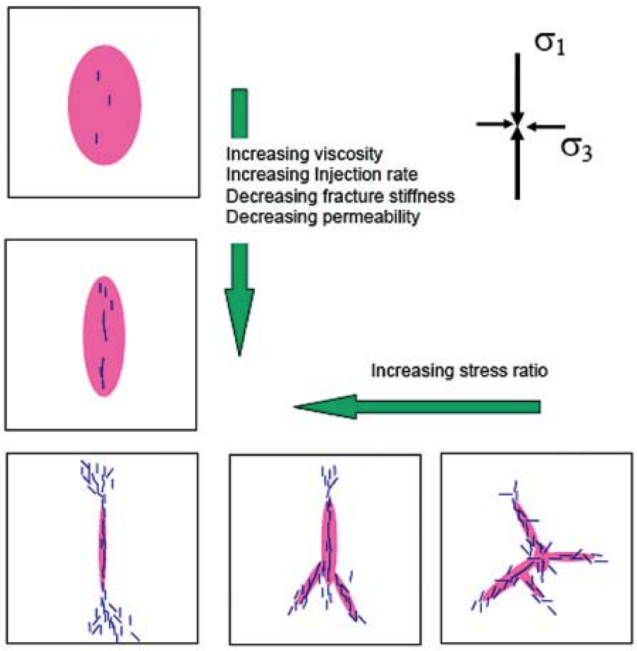

Figure 2.2: Schematic diagram showing fluid (pink ellipses) and fracture (blue lines) behavior with respect to local stress regimes. For decreasing stress ratio, fractures open and propagate in random orientations [35].

principal stress (σ_3) directed along the horizontal direction. This design will be subjective to rigorous testing in our simulations. At Rosemanowes, United Kingdom, [34, 25] the reservoir was engineered to have a large network of micro-cracks, fissures and fractures but only a limited number of major fractures accounted for most of the flow. The EGS project at Soultz-sous-Forêts, France [1, 10] has a system of interconnected faults and large-scale fractures. All three configurations are depicted in Figure 2.3.

Several important outcomes of these international research projects that improved our understanding of the engineered reservoirs in response to stimulation are highlighted here. These should be considered as guidelines for carrying out the numerical simulations.

- There exist three-dimensional networks of hydraulically activated joints and fractures in all EGS reservoirs that account for the hydraulic connection between injection and production wells.
- Shearing of already existing joints that are aligned favorably to local stress field is the main mechanism behind reservoir growth. Fractures are not formed through tension but they rather fail when pumping pressure exceeds the critical pressure for shear failure.

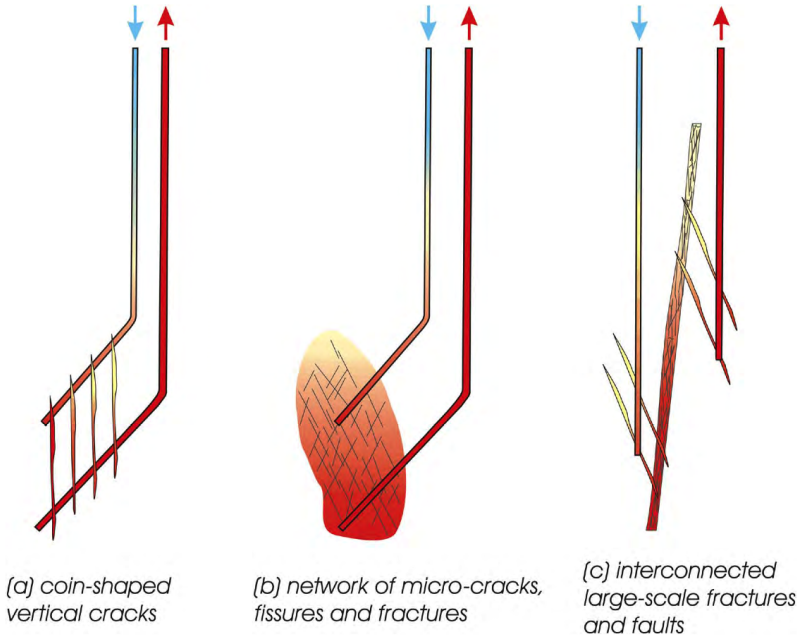

Figure 2.3: Fracture and subsurface heat exchanger configurations for EGS at a) Fenton Hill (New Mexico), b) Rosemanowes (United Kingdom) and c) Soultz-sous-Forêts (France) [15].

- Too high pumping pressures can cause a runaway reservoir growth resulting in water losses. Overstimulation can cause short-circuiting between wells resulting in lower production temperature.
- Very high flow rates with long paths ensuring minimum residence time for injected water are preferred [39].

2.5 Challenges for Successful Stimulation

EGS studies have shown a tremendous scope of improvement in terms of reservoir productivity by means of stimulation and fracture engineering. Yet the production flow rates have not reached a stage where EGS projects become economically attractive to decision makers of a nation. Limited subsurface knowledge and inaccessibility to rock volume make the problem more challenging. As the projects extend beyond prior experience, numerical modelling assists in studying the long-term response of EGS reservoirs towards stimulation. In this master's thesis, different geometric layouts and arrangements of engineered fractures are compared and optimized with respect to their heat recovery efficiency.

Chapter 3

Numerical Modelling

SHEMAT (**S**imulator for **HE**at and **MA**ss **T**ransport) is a reactive transport code for simulating steady-state and transient processes in hydrothermal reservoirs in two and three dimensions. It solves coupled problems involving fluid flow, heat transfer, species transfer and chemical water-rock interaction in fluid saturated porous media. It is designed to handle a range of time scales, from technical to geological processes and can address the long-term behavior of heat mining installations like EGS [14].

3.1 Governing Equations

To carry out the simulations, forward modelling code SHEMAT is implemented via the graphical user interface Processing SHEMAT. The partial differential equations governing the fluid flow and heat transport are derived from conservation of mass, momentum and energy. SHEMAT solves these equations by a finite difference method. Momentum conservation is expressed by Darcy's law which describes the groundwater flow in a confined aquifer as:

$$\boldsymbol{v} = -\frac{\underline{k}}{\mu_f}(\nabla P + \rho_f \cdot g \cdot \nabla z) \tag{3.1}$$

where $\boldsymbol{v}$ is the specific discharge (or Darcy velocity) ($\mathrm{m\,s^{-1}}$), $\underline{k}$ is the hydraulic permeability tensor ($\mathrm{m^2}$), μ_f is the fluid dynamic viscosity ($\mathrm{Pa\,s}$), P is the hydraulic pressure (Pa), ρ_f is the fluid density ($\mathrm{kg\,m^{-3}}$), g is the gravity ($\mathrm{m\,s^{-2}}$) and z is the depth (m) [14]. The equivalent hydraulic head h_0 (m) and measured hydraulic head h (m) are given as:

$$h_0 = \frac{P}{\rho_0 \cdot g} + z_d \tag{3.2}$$

$$h = \frac{h_0 \cdot \rho_0}{\rho_f} \tag{3.3}$$

where ρ_0 is the reference density ($\mathrm{kg\,m^{-3}}$) and ρ_f is the fluid density that is constant over depth ($\mathrm{kg\,m^{-3}}$) [26].

Corresponding pore water pressure is calculated by distribution of equivalent hydraulic head h_0 (Eq.(3.2)) and depth z_d as :

$$P(z_d, h_0) = P_0 + \int_0^{z_d} \rho_f(z_d) \cdot g(h_0 - z_d) \cdot dz_d \tag{3.4}$$

where $P_0(z_0) \approx 10^5\,\mathrm{Pa}$ is the pressure at the surface $z_d = 0$ [41].

Continuity equation expresses the conservation of mass as:

$$0 = \partial(\phi \cdot \rho_f)/\partial t + \nabla(\rho_f \cdot \boldsymbol{v}) \tag{3.5}$$

where ϕ is the porosity.

The equation implemented in SHEMAT for fluid flow is derived from Eqs.(3.1), (3.4) and (3.5) using the Oberbeck-Boussinesq approximation [33, 9]:

$$\rho_f \cdot g(\alpha + \phi \cdot \beta)\frac{\partial h}{\partial t} = \nabla[\frac{\rho_f \cdot g \cdot \underline{k}}{\mu_f}(\nabla h_0 + \rho_r \cdot \nabla z)] + W \tag{3.6}$$

where α and β are the compressibility ($\mathrm{Pa^{-1}}$) of the rock and the fluid phase respectively. W denotes the mass source term ($\mathrm{kg\,m^{-3}\,s^{-1}}$) [41].

The heat transport equation is obtained from conservation of energy [14]:

$$(\rho \cdot c)_e \frac{\partial T}{\partial t} = \nabla(\underline{\lambda_e} \cdot \nabla T - (\rho \cdot c)_f \cdot T \cdot \mathbf{v}) + H \tag{3.7}$$

where $(\rho c)_e$ is the effective volumetric heat capacity of the saturated porous medium and the fluid ($\mathrm{J\,m^{-3}\,K^{-1}}$), T is the temperature (°C), $(\rho c)_f$ is the heat capacity of the fluid ($\mathrm{J\,m^{-3}\,K^{-1}}$), $\underline{\lambda_e}$ is the tensor of effective thermal conductivity ($\mathrm{W\,m^{-1}\,K^{-1}}$) and H is the heat generation rate source term ($\mathrm{W\,m^{-3}}$).

There is a non-linear coupling between Eqs.(3.6) and (3.7) as pressure and temperature influence the physical properties of the rock matrix and the fluid. Transfer of heat takes place by advection and conduction in the porous media neglecting the contribution of thermal dissipation, radiation and dispersion [14].

3.2 Model Geometry

In this section, model architecture is introduced along with the spatial distribution of its thermal, hydraulic and mechanical properties. A vertical model with a number of cross sections is chosen to represent the reservoir volume. It is

preferred over a model with horizontal layers as it better suits the task at hand of simulating vertically aligned fracture zones in the subsurface rock. SHEMAT uses a block-centered grid whose nodes are located at the center of grid cells. The numerical grid comprises of 35 x 49 x 111 cells. Having a coarser grid (with cell dimensions as 300 m x 100 m x 20 m) results in loss of essential details while extremely fine computation grid (with cell dimensions as 10 mm x 100 m x 20 m) is numerically unstable and time consuming. The cell dimensions vary from 1 m - 160 m, 10 m - 100 m, 20 m - 160 m in x-, y-, and z- directions respectively (where z is pointing vertically upward). Grid is refined near the injection and production wells to accommodate for the higher fluid velocities at these wells. This grid discretization is adopted after testing several models with varying grid cell sizes. The model thus represents a trade off between conflicting goals of achieving numerical stability and reasonable computing times while preventing loss of relevant details. The model properties are given in Table 3.1.

Table 3.1: Properties of the SHEMAT model.

Parameter	**Value**
Grid size	35 x 49 x 111
Number of nodes	190356
Model extent	1271 m x 3020 m x 3100 m
Temperature at top	150 °C
Hydraulic head at top	4000 m
Basal heat flow	0.08 W m^{-2}
Constant water density	862 kg m^{-3}

The maximum principal horizontal stress (σ_1) is considered along the y-direction and the minimum principal horizontal stress (σ_3) is along the x- direction (Fig. 3.1). As discussed in Section 2.3, this facilitates opening and propagation of fractures in x- and y- directions respectively. The low porosity crystalline (granite) reservoir is considered in a depth range between 4000 m - 7100 m with a temperature of 150 °C at the top. A basal heat flow of 0.08 W m^{-2} marks the lower boundary condition of the reservoir. The model consists of five property zones with different permeability and porosity values, while thermal capacity and thermal conductivity remain the same for all the zones. Zone 1 (top zone) starting at a depth of 4000 m has a thickness of 560 m overlying 1980 m thick Zone 2 (middle zone), followed by 560 m thick Zone 3 (bottom zone) as the basement. All three zones extend over the entire length and width of the reservoir. Zone 4 (surrounding zone), oriented along the direction of maximum principal horizontal stress (σ_1) lies within Zone 2 with a width of 31 m. It has a higher porosity and permeability than Zones 1-3. The actual fracture zone, i.e. Zone 5 is enclosed within the surrounding zone along the y- direction and has a width of

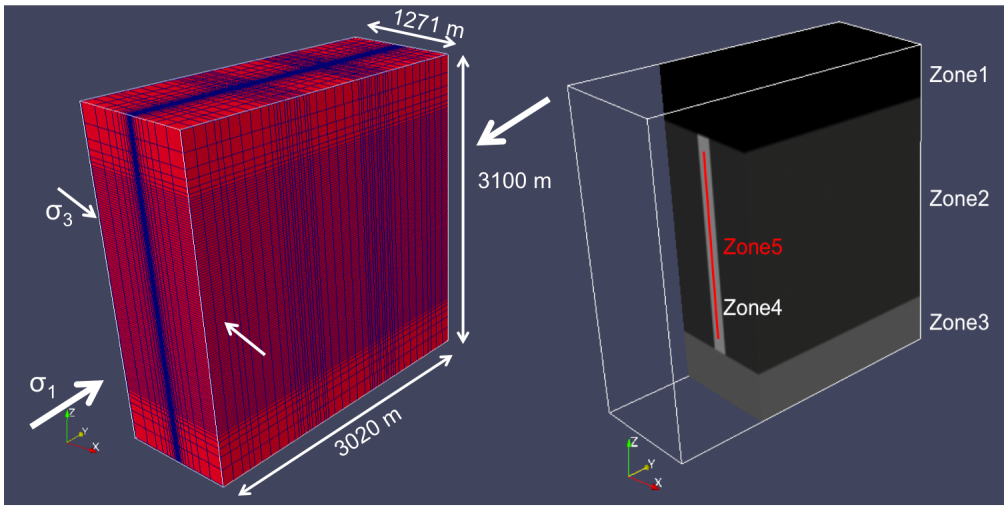

Figure 3.1: Numerical grid, stress regime and property zones defined in the SHEMAT model. Fracture zone (not to scale) is shown in red on the right.

1 m. It is highly permeable and porous. Zone 4 and Zone 5 are the regions where most of the injected fluid circulates (Fig. 3.1). The heights of these two zones should be large enough to provide enough area for fluid circulation, otherwise the injected fluids will follow a direct shorter path to the production well without heating up properly. The surrounding zone is 1980 m high and the fracture zone is 1620 m high. Fracture apertures lie in the range of 3 mm - 10 mm for low-to-medium permeability formations [18]. An attempt is made to simulate the fracture zone with a width of 5 mm having an extremely high porosity of 95 % (equivalent of a large frac with 5 mm aperture) but it is numerically unstable. Therefore, a width of 1 m is chosen for the fracture zone with a porosity of 0.5 % which would be equivalent of having large number of small fractures with 5 mm aperture. Properties of different zones are given in Table 3.2.

Table 3.2: Thermal and hydraulic properties of different property zones.

Parameter	**Zone1**	**Zone2**	**Zone3**	**Zone4**	**Zone5**
Porosity	0.001	0.001	0.001	0.002	0.005
Permeability (m^2)	10^{-18}	10^{-19}	10^{-20}	10^{-15}	10^{-11}
Thermal capacity ($MJ\,m^{-3}\,K^{-1}$)	2.1	2.1	2.1	2.1	2.1
Thermal conductivity ($W\,m^{-1}\,K^{-1}$)	2.7	2.7	2.7	2.7	2.7
Rock compressibility (Pa^{-1})	10^{-10}	10^{-10}	10^{-10}	10^{-10}	10^{-10}

3.3 Simulation and Results

To start with, a steady-state simulation is performed to obtain an undisturbed temperature field using the Il'in flux blending scheme [14] with coupled rock thermal properties. This temperature field is then fed as an input into the transient coupled heat and fluid flow simulation. Next, the time parameters for the transient simulation are defined (Table 3.3). Total simulation time is composed of 6 stress periods, each divided into 20 time steps. The length of periods vary from 1 month (30 days) to 15 years (5475 days), summing up to 31.58 years (11527 days). There is a coupling between flow and heat transport. Flow depends on heat transport via the temperature dependence of the fluid density, viscosity and compressibility. Heat transport depends on flow in case of advection heat transfer via the pressure dependence of fluid thermal conductivity and fluid volumetric thermal capacity. These fluid properties are calculated and updated simultaneously during the numerical simulations [14]. As Processing SHEMAT only allows to input volumetric flow rates at injection and production wells, the density of injected water is set to a constant value of $862\,\mathrm{kg\,m^{-3}}$ (at temperature = 200 °C and salinity = $0\,\mathrm{mg\,L^{-1}}$ [32]). If the water density is not kept constant, it varies by around 15 % over the simulation time with varying temperature. As this density variation causes a mass difference between the water injected and produced at different temperatures, hydraulic head will increase continuously. Therefore, this mass difference is avoided in the simulations by fixing water density at a constant value.

Table 3.3: Time parameters for the transient simulation.

Stress Period	**Length (years)**	**Time steps**
1	0.0834	20
2	0.5	20
3	1	20
4	5	20
5	10	20
6	15	20

A doublet is introduced with the injector (injection well) and producer (production well) placed 1200 m apart in the fracture zone at depths of 5550 m (model depth of 1550 m) and 5350 m (model depth of 1350 m) respectively. Water is injected at a temperature of 80 °C with a constant flow rate of $50\,\mathrm{L\,s^{-1}}$ ($0.05\,\mathrm{m^3\,s^{-1}}$) at the injector and produced at higher temperatures with the same flow rate (assuming 100 % fluid recovery from the reservoir) from the producer. The development of bottom-hole temperature at the producer and the resultant 'penny-shaped' heat-exchange area from the simulation are shown in Fig. 3.2

and 3.3 respectively. Temperatures decrease uniformly over time as the reservoir gets cooler by the heat extraction. A slight bump in the temperature curve is noticed at the beginning ($\sim$ first 200 days). As the producer is located 200 m above the injector, it produces colder water before warmer water reaches there. The continuous injection and production of geothermal fluids result in a pressure increase at the injector and a pressure decrease at the producer over time.

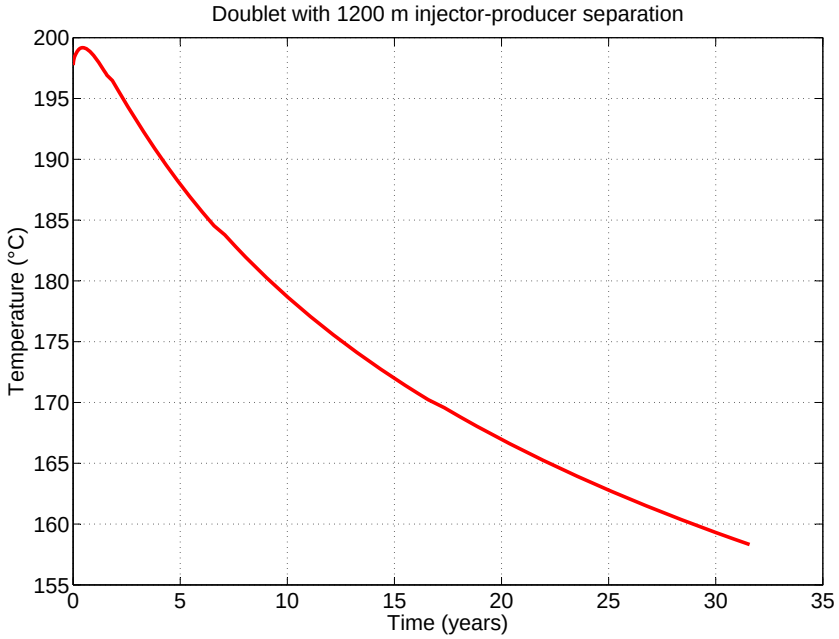

Figure 3.2: Bottom-hole temperature for the producer at a flow rate of $50\,\mathrm{L\,s^{-1}}$.

3.4 Doublet Optimization

Before the model from Section 3.3 is adapted to accommodate a triplet (1 injector, 2 producers) or multiple doublets and triplets, there are several parameters that need to be optimized for efficient heat recovery. Reservoir performance is sensitive to number of factors like horizontal separation between injector-producer, production flow rate, fracture zone permeability and number of time steps used in the transient simulation. These factors influence the temporal development of bottom-hole temperatures and heat exchange areas in the reservoir. A comprehensive study is done here where these parameters are varied systematically and their effects are observed.

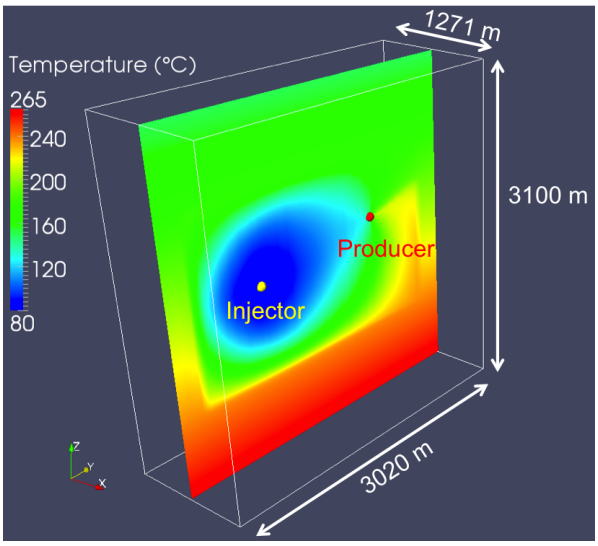

Figure 3.3: Cross section along σ_1 showing 'penny-shaped' heat exchange area created by water circulation at a flow rate of $50\,\mathrm{L\,s^{-1}}$ after 31 years.

3.4.1 Injector - Producer Separation

On the surface, wells are usually drilled next to each other separated by a few meters only, whereas the bottom holes in the deeper sections of the reservoir are placed a few hundred meters apart [21]. Permeabilities of $10^{-11}\,\mathrm{m^2}$ and $10^{-15}\,\mathrm{m^2}$ are defined for the fracture and surrounding zones respectively in Section 3.2. Permeability is a rock property but transmissivity on the other hand is highly influenced by injection flow rates and well design. Transmissivity includes the cross-sectional area where the fluid circulation takes place absorbing heat from the reservoir. Thus, it makes sense to increase the separation between wells while aiming for higher transmissivities [39]. While a very large separation results in a significant pressure drop and inefficient heat mining from the reservoir, the chances of a short-circuit between the wells get higher if their bottom holes are located close to each other. In the latter scenario, the injected geothermal fluids do not get enough residence time to extract heat from the surrounding rocks and they reach the producer quickly. It results in lower production temperatures and render an EGS project uneconomical and unviable. Therefore the separation between the injector and the producer in the subsurface needs to be optimized.

Four different models are created with increasing separation (600 m, 800 m, 1000 m and 1200 m) between the injector and producer while keeping the other parameters same. Thermal drawdown from different models is shown in Fig. 3.4. A very low separation of 600 m gives a sudden temperature decline. For 800 m and 1000 m separations, bottom-hole temperatures plummet down to 160 °C after 12 and 19 years respectively. For 1200 m separation, bottom-hole temperatures

decrease uniformly giving a 20 % decline over 31 years, thereby establishing the system as economical. As shown in Fig. 3.5, the pressure drop increases with separation; reaching up to 2.1 MPa for 1200 m separation which is reasonable. Thus the separation is fixed as 1200 m for further models. The growth of heat-exchange areas for different separations is visualized in Fig. 3.6.

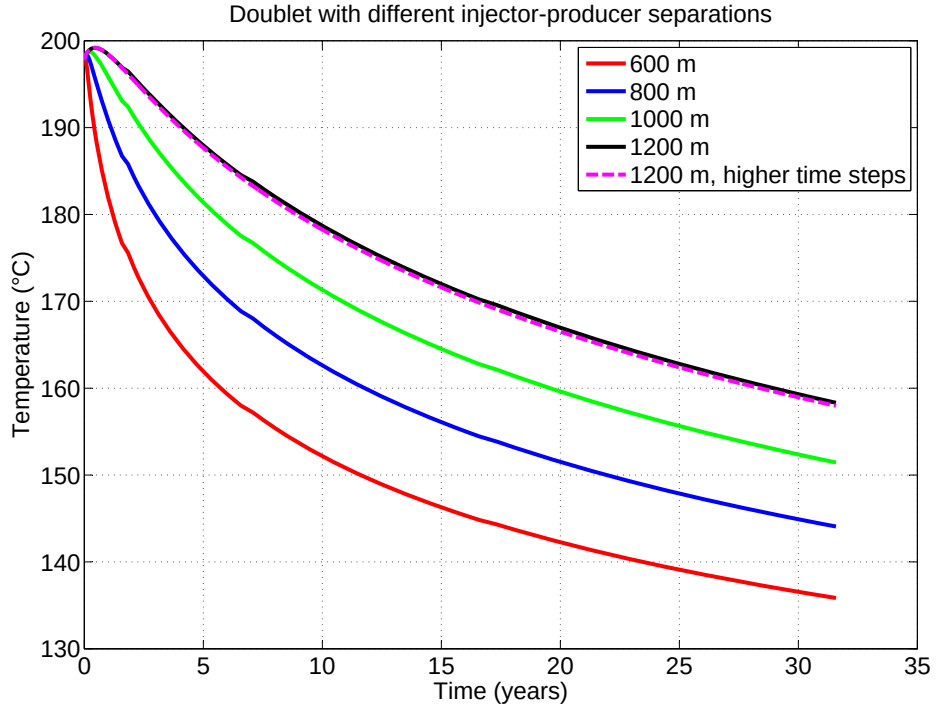

Figure 3.4: Bottom-hole temperatures for the producer at a flow rate of 50 L s^{-1}. Also shown is the temperature development with increased time steps.

Initially, the model is run with only 120 time steps. When run again with 1595 time steps (Table 3.4), the simulation takes 12 times longer than the initial run and still gives exactly the same result (Fig. 3.4). This shows that 120 time steps are adequate to obtain a stable result while saving simulation runtime. Simulations are carried out on 12 Intel® Xeon® X5690 3.47 GHz processors.

3.4.2 Flow Rates

Economic feasibility of an EGS reservoir can not be ensured unless the production flow rates are high enough. While hydrocarbon fuels release stored chemical energy on combustion, same is not the case for geothermal fluids as only their sensible and latent enthalpy are used. In order to be comparable in terms of energy content with an oil well, a geothermal well has to produce hot water with high mass flow rates. Higher flow rates are only possible if the reservoir trans-

Table 3.4: Time parameters with increased time steps.

Period	Length (years)	Time steps
1	0.0834	20
2	0.5	25
3	1	50
4	5	250
5	10	500
6	15	750

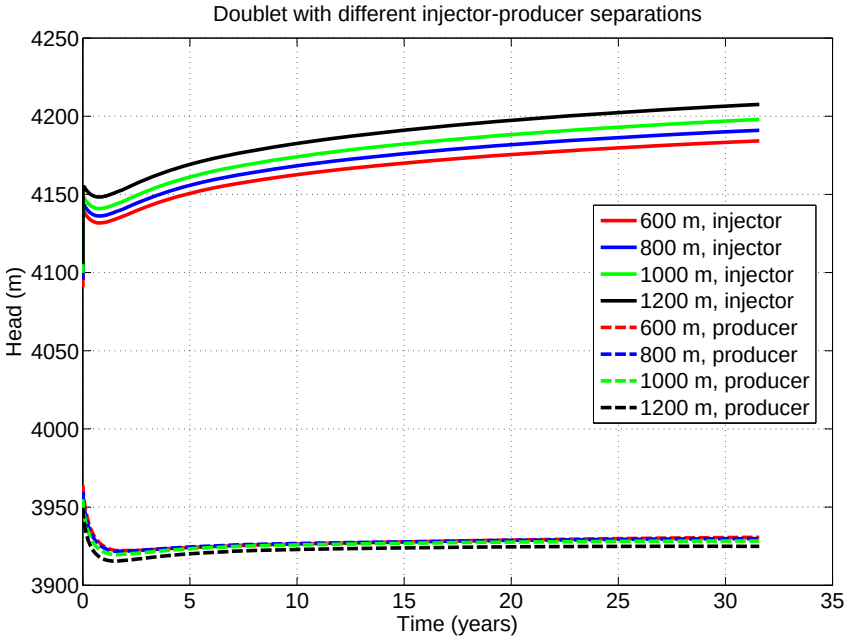

Figure 3.5: Hydraulic heads for the injector and the producer at a flow rate of $50\,\mathrm{L\,s^{-1}}$.

missivity is high which has already been achieved by placing the wells 1200 m apart in Section 3.4.1. At the same time, re-injected colder water must get sufficient residence time to reheat to formation temperatures. It should be kept in mind that very high injection pressures can be counterproductive too in two ways. Firstly, they can cause short-circuiting between the wells and secondly, they can extend the reservoir by exceeding the critical pressure beyond which the fractures grow. The latter situation would result in fluid loss to non-circulating parts of the reservoir and a reduction in effective heat-transfer area. This was the case at Fenton Hill, where high-injection pressures led to the growth of fractured volume in regions that were not accessible by the wells [39].

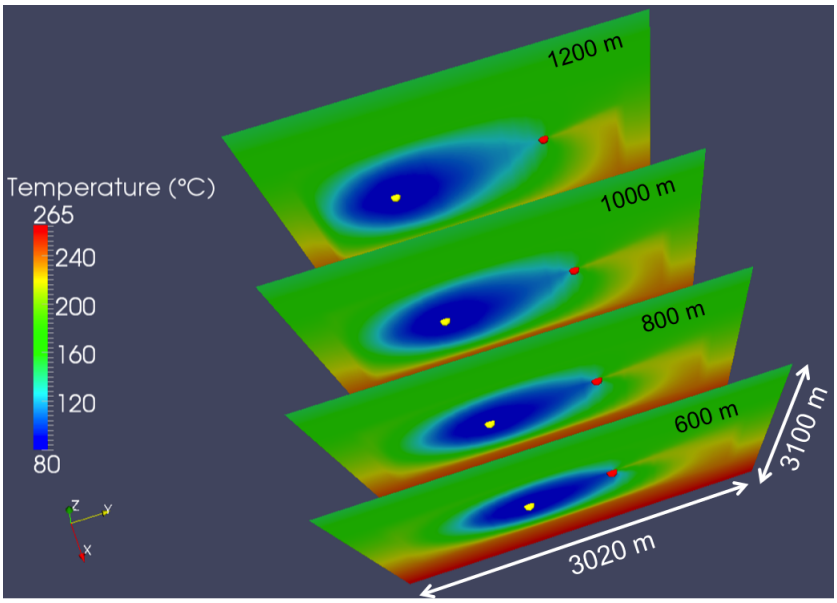

Figure 3.6: Cross sections along σ_1 depicting the increase in heat-exchange area with increasing injector - producer separation at a flow rate of $50\,\mathrm{L\,s^{-1}}$ after 31 years. Yellow and red spheres represent the injectors and the producers respectively.

Six models are created where water is circulated at different volumetric flow rates (constant over time) between wells placed 1200 m apart. The bottom-hole temperatures at the producer are shown in Fig. 3.7 for different flow rates. A very low flow rate of $10\,\mathrm{L\,s^{-1}}$ ($0.01\,\mathrm{m^3\,s^{-1}}$) does not give any temperature decline over 31 years and hence can be considered as a sustainable system. Here, the residence time of the circulating fluid is adequately large to extract the thermal energy from the reservoir efficiently, but the flow rate is very small to make an EGS system economical. Flow rates of $20\,\mathrm{L\,s^{-1}}$ - $40\,\mathrm{L\,s^{-1}}$ give a thermal drawdown between 10 °C - 30 °C over 31 years, nevertheless the heat-exchange areas are rather small (Fig. 3.8). High flow rate of $50\,\mathrm{L\,s^{-1}}$ gives a temperature drawdown of 40 °C while having a large heat-exchange area. A rapid decline in bottom-hole temperatures is observed at relatively short times at a very high flow rate of $100\,\mathrm{L\,s^{-1}}$, undoubtedly caused by a short-circuit between the wells. Fig. 3.9 shows thermal power P_t of a doublet operating at different flow rates. For flow rates above $50\,\mathrm{L\,s^{-1}}$, the average thermal power increases by around $3\,\mathrm{MW}_t$ and average electrical power by $0.3\,\mathrm{MW}_e$ for every $10\,\mathrm{L\,s^{-1}}$ increase. Clearly, thermal power of EGS reservoirs can be increased by having higher production flow rates provided that it does not result in premature cooldown. A constant flow rate of $50\,\mathrm{L\,s^{-1}}$ serves as the best way to achieve efficient heat mining from the reservoir with less fluid circulation costs while avoiding a short-circuit.

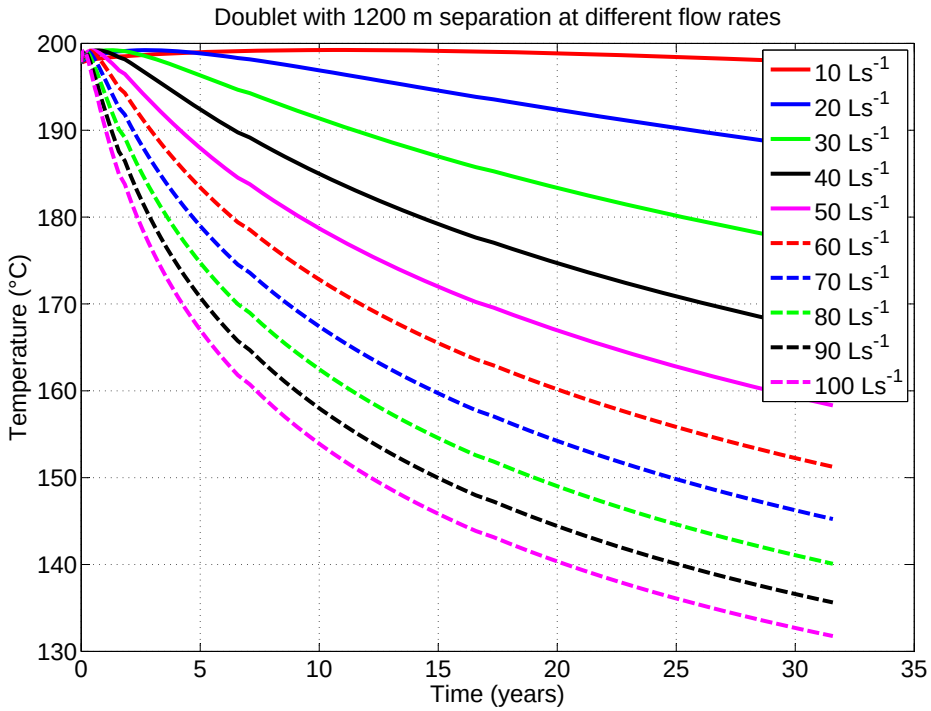

Figure 3.7: Bottom-hole temperatures for the producer with increasing flow rates.

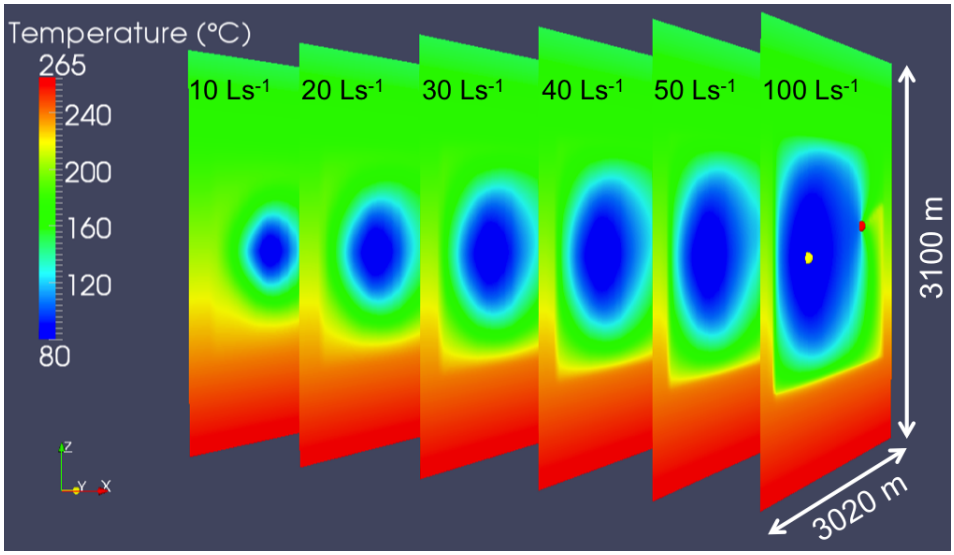

Figure 3.8: Cross sections along σ_1 depicting the increase in heat-exchange area with increasing flow rates. Yellow and red spheres represent the injector and the producer respectively.

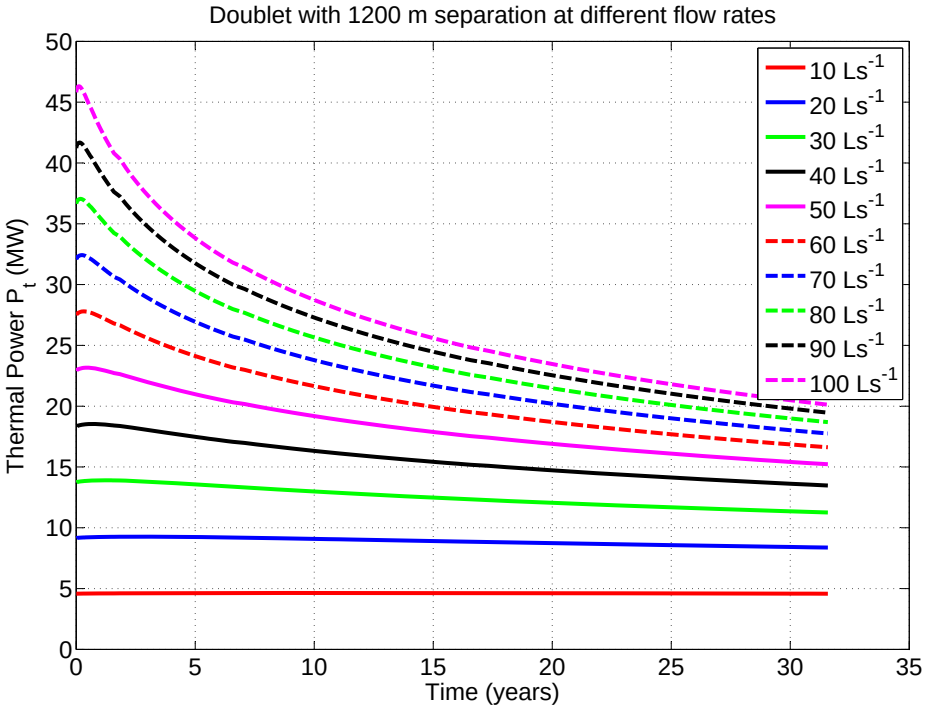

Figure 3.9: Thermal power P_t of a doublet with increasing flow rates.

3.4.3 Permeability of Fracture Zone

[19] define the permeability of fractured igneous and metamorphic rocks in the range of $10^{-11}\,\mathrm{m}^2$ to $10^{-15}\,\mathrm{m}^2$. A value of $10^{-11}\,\mathrm{m}^2$ is assigned to the fracture zone in the SHEMAT models after rigorous testing. This section explains the reasoning behind choosing this value. At a constant injection flow rate of $50\,\mathrm{L\,s}^{-1}$, temperature and hydraulic head development are compared in Fig. 3.10 and 3.11 for four different models where fracture zone permeabilities vary between $10^{-11}\,\mathrm{m}^2$ - $10^{-13}\,\mathrm{m}^2$ with decreasing order of magnitude. A very high permeability of $10^{-10}\,\mathrm{m}^2$ gives a temperature decline of $40\,^{\circ}\mathrm{C}$ over 31 years while both injector and producer have similar hydraulic heads. Permeability of $10^{-11}\,\mathrm{m}^2$ gives similar temperature development with a hydraulic head difference in the order of several hundred meters between the wells. A further decrease in permeability to $10^{-12}\,\mathrm{m}^2$ results in lower temperature decline but hydraulic heads differ by several thousand meters. Very low permeability of $10^{-13}\,\mathrm{m}^2$ gives very high bottom-hole temperatures and hydraulic heads differ by tens of thousands of meters. To understand, how these head developments influence an engineered geothermal system, the concept of flow resistance is introduced.

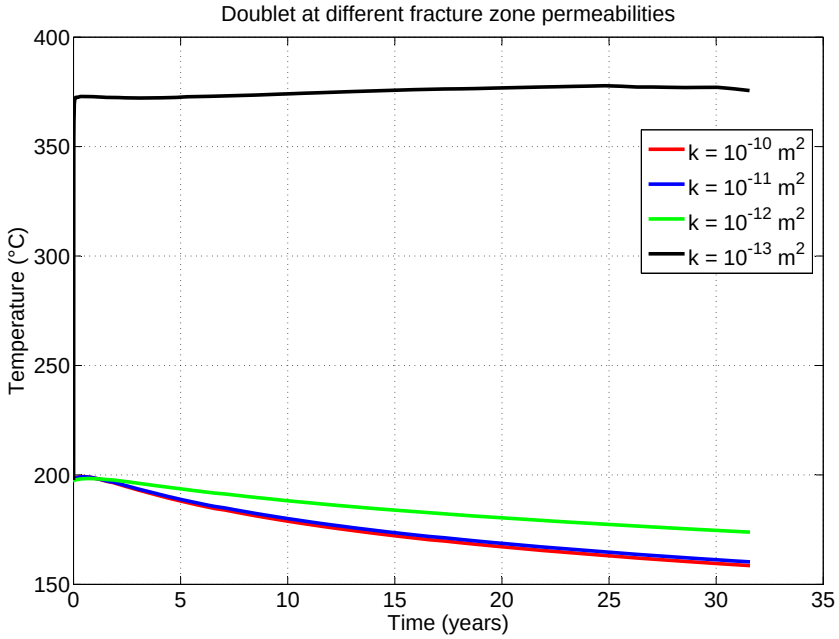

Figure 3.10: Bottom-hole temperatures for the producer with decreasing fracture zone permeability at a flow rate of $50\,\mathrm{L\,s^{-1}}$.

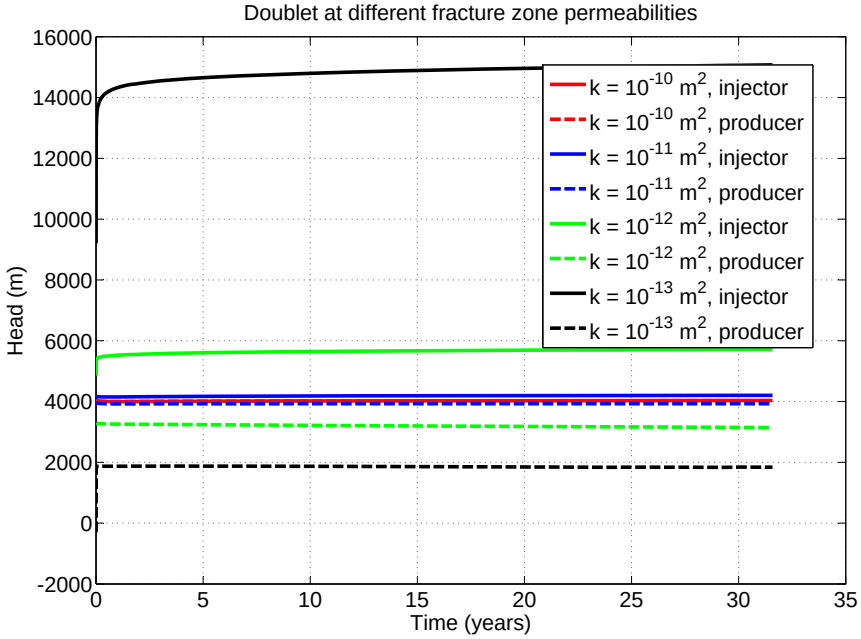

Figure 3.11: Hydraulic heads for the injector and the producer with decreasing fracture zone permeability at a flow rate of $50\,\mathrm{L\,s^{-1}}$.

[15] outlines several minimum requirements which are essential for a commercially successful EGS installation. Ensuring that flow resistance, or *reservoir impedance* i of an EGS stays within the threshold of $100\,\mathrm{kPa\,s\,L^{-1}}$ is one of them. Defined as the pressure drop between the injection and production wells divided by the production flow rate, it can be understood as the pressure difference necessary to circulate a certain fluid volume [25].

$$i = \frac{\bar{p}_{injection} - \bar{p}_{production}}{Q} \tag{3.8}$$

where $\bar{p} = \bar{h} g \rho_w$ is the average pressure (Pa) in the injection or production borehole and Q is the volumetric flow rate ($\mathrm{L\,s^{-1}}$).

Considering a flow rate of $50\,\mathrm{L\,s^{-1}}$, the reservoir impedance values for different fracture zone permeabilities are given in Table 3.5. On comparing the values, only the fracture zone permeability of $10^{-11}\,\mathrm{m^2}$ gives a reservoir impedance below $100\,\mathrm{kPa\,s\,L^{-1}}$, thereby justifying the decision of defining this permeability value for the fracture zone.

Table 3.5: Reservoir impedance at different fracture zone permeabilities.

Permeability ($\mathrm{m^2}$)	**Reservoir Impedance ($\mathrm{kPa\,s\,L^{-1}}$)**
10^{-10}	-0.06
10^{-11}	40.22
10^{-12}	391.17
10^{-13}	2109.93

3.4.4 Width of Surrounding Zone

The extent of fluid circulation in an EGS reservoir differs from site to site around the world and depends on the region's tectonic history and stress regimes that govern the spread of existing fractures. For example, the natural fracture network extends over thousands of meters in Soultz-sous-Forêts reservoir [41]. Since this extent is unknown in our model, different widths of the surrounding zone are simulated in SHEMAT models to see how much volume is being accessed by the circulating geothermal fluids. The width of the surrounding zone in our models may appear trivial for a single doublet or triplet, but it becomes a vital parameter that requires optimization when multiple doublets or triplets are drilled in the reservoir next to each other.

Three models are run with widths of surrounding zone as 31 m, 151 m and 311 m. Increasing the surrounding zone (Zone 4) width results in marginal reduction in thermal drawdown for the same doublet as the *heat-transfer volume*

(portion of reservoir volume accessible by the circulating fluids [11]) increases with width. Looking at the slices from three different models in Fig. 3.12, it is clear that the heat-transfer volume is the highest at the depth of fluid injection. Irrespective of the increase in width of surrounding zone, the heat-transfer volume becomes more or less constant for the regions above and below the injection point at a given flow rate. For the following simulations involving a single doublet or a triplet, a width of 311 m is set for the surrounding zone.

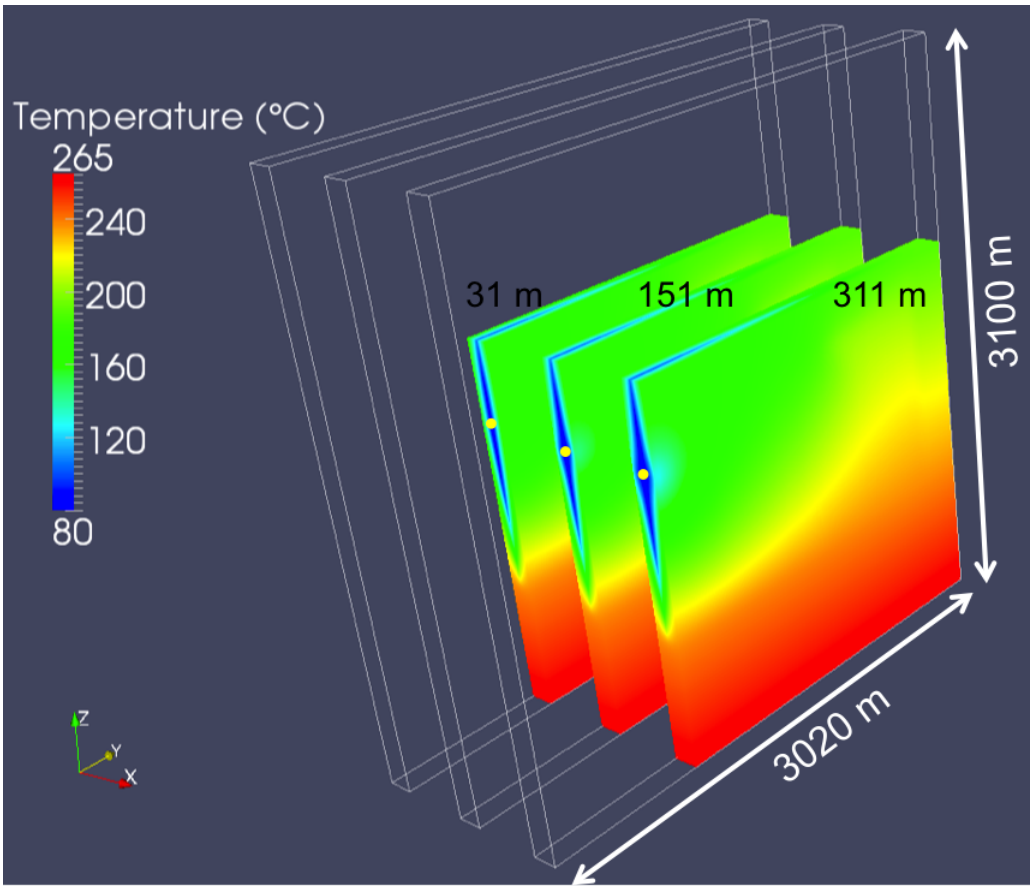

Figure 3.12: Slices of same width along σ_1 from three different models depicting the heat-transfer volumes for increasing width of surrounding zone. Yellow spheres represent the injectors.

3.5 Triplet

It is a common practice in EGS projects, for example at Soultz-sous-Forêts and Rosemanowes to have more than one producer on both sides of the injector to produce hot geothermal fluids while the central injection borehole re-injects the used geothermal fluids back into the subsurface. Such a setup has a much larger heat-exchange area and extracts more thermal energy from the reservoir at the expense of an extra borehole. [23] says that drilling costs for boreholes rise exponentially with depth and account for majority of the initial investment. Though requiring a higher initial investment, a triplet produces a lot more energy over time when compared to a doublet. A detailed economic evaluation of Engineered Geothermal Systems has numerous physical and financial dependencies and is beyond the scope of this study. The key focus here is to optimize the process of heat production from an EGS reservoir without any budgetary considerations.

To accommodate a second producer, the starting model from Section 3.2 is extended along the direction of maximum principal horizontal stress (σ_1) while keeping the thermal and hydraulic parameters as the same. At first, the triplet is simulated with a constant injection rate of $50\,\mathrm{L\,s^{-1}}$ with two wells producing at a rate of $25\,\mathrm{L\,s^{-1}}$ each. Over 31 years, a doublet gives a thermal drawdown of 40 °C while a triplet gives a thermal drawdown of only 25 °C, but that is not important here. The fact that geothermal fluids are being produced at half the flow rates from two producers is more relevant. Extension of a doublet to a triplet at the same injection flow rate corresponds to a minor increase in average electrical power and produced thermal energy over time. But, on simulating the triplet with a constant injection rate of $100\,\mathrm{L\,s^{-1}}$, a substantial increase in thermal energy is achieved. Average thermal and average electrical power increase by $20\,\mathrm{MW}_t$ and $2\,\mathrm{MW}_e$ respectively on doubling the injection flow rate. To summarize, a triplet allows us to have higher injection flow rates without causing a short-circuit and yet produce more energy than a doublet.

If a triplet is reversed to have one producer in the center and two injectors on the sides, a slight increase in average thermal power is observed. Reversing the triplet increases the spread of heat-exchange area but with less efficient heat extraction. As shown in Fig. 3.13, reservoir is not cooled properly in the regions surrounding the central producer. Choosing between a triplet or a reversed triplet is more of a concern when multiple instances of them are installed next to each other in the reservoir. Making that choice has huge impact on the well field area and it will be studied in the next section.

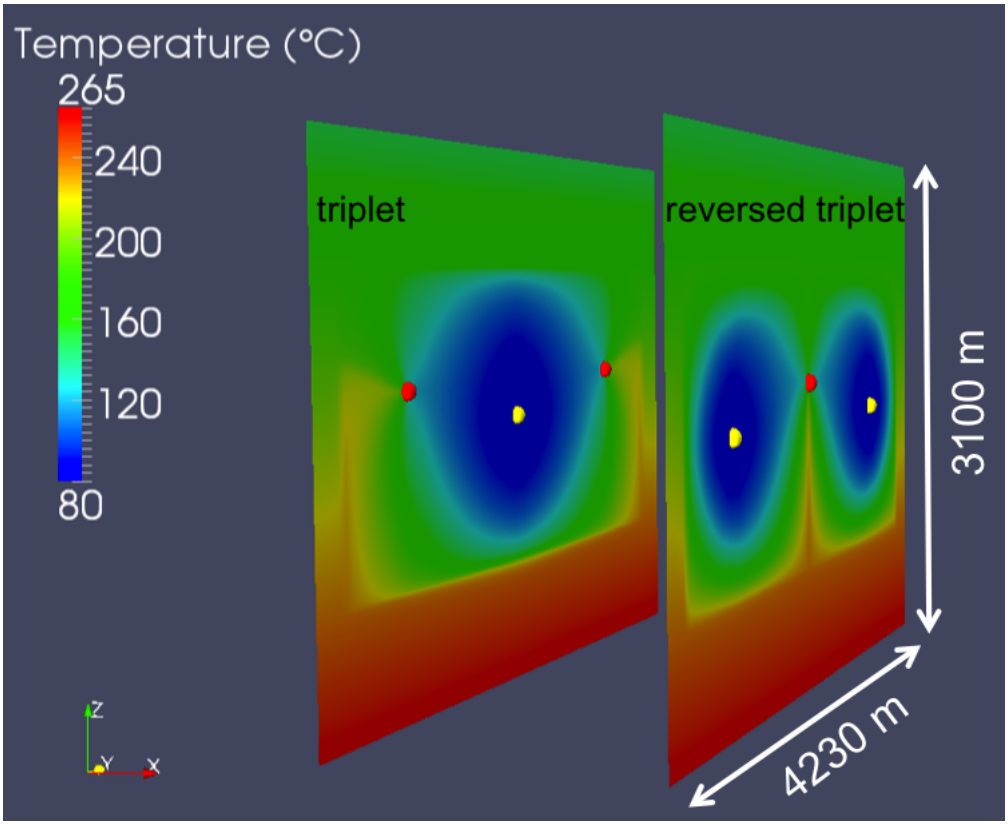

Figure 3.13: Cross sections along σ_1 depicting heat-exchange areas created by triplet and reversed triplet. Yellow and red spheres represent the injectors and the producers respectively.

3.6 Modularity of EGS

A big advantage of Engineered Geothermal Systems over other renewable energy sources (wind, hydropower, solar photovoltaics) is their modularity. In a reservoir, more than one doublet or triplet can be implemented next to each other, thereby making EGS scalable from 10^0 MW_e - 10^2 MW_e. Their ability to cogenerate heat and power makes them versatile and allows easy deployment for large-scale applications like district heating and base-load power supply with capacity factors above 90 % [3]. Among all electricity production technologies, geothermal systems have the second lowest land footprint [28]. Heat to power conversion plants on the surface along with the cooling towers and auxiliary buildings are relatively compact. They are usually located at or near the geothermal reservoir to avoid any temperature and pressure drop over long transmission lines. The well fields can take up to 5 km^2 - 15 km^2 of area but the well pads at the surface only account for 2 % of the area. The remaining surface area can support farming, grazing or fisheries. Advanced directional drilling techniques allow multiple wells to be drilled from the same pad thus minimizing the total wellhead area [39]. So far, only one vertical fracture zone along maximum principal horizontal stress (σ_1) has been simulated with a doublet or a triplet. To extend the accessible rock volume, this study proposes a layout to engineer three vertically oriented fracture zones each with its own wells. And numerical modelling helps to determine the optimum separation between these fracture zones.

3.6.1 Multiple Doublets

The starting model from Section 3.2 is extended to accommodate 3 fracture zones (Zone 5) encompassed by one common surrounding zone (Zone 4) in the reservoir. Each fracture zone has two doublets located along the y- direction. With injectors (1 and 4) on the outskirts, the producers (2 and 3) are located in the middle at a separation *s1* of 300 m (Fig. 3.14 and 3.15). Now consider 3 such zones aligned parallel to each other at a separation *s2* of 300 m along the x-direction. *s1* corresponds to the separation between the producers of the same fracture zone, while *s2* corresponds to the separation between producers of the adjacent fracture zones. Both these separations are decreased simultaneously in steps of 50 m.

Five different models are considered where *s1* = *s2* = {100, 150, 200, 250, 300} m. The models are run for 31 years with a constant injection flow rate of 50 L s^{-1}. For separations of *s1* = *s2* = {150, 200, 250, 300} m, all six producers (2, 3, 6, 7, 10 and 11) give similar thermal drawdown of 40 °C with slightly lower bottom-hole temperatures in the central producers (6 and 7). This difference of around 1 °C means that the *heat-transfer volumes* of the adjacent doublets start to overlap thereby cooling the reservoir effectively. When the separation *s1* = *s2* = 100 m, the temperature difference after 31 years between central (6 and 7)

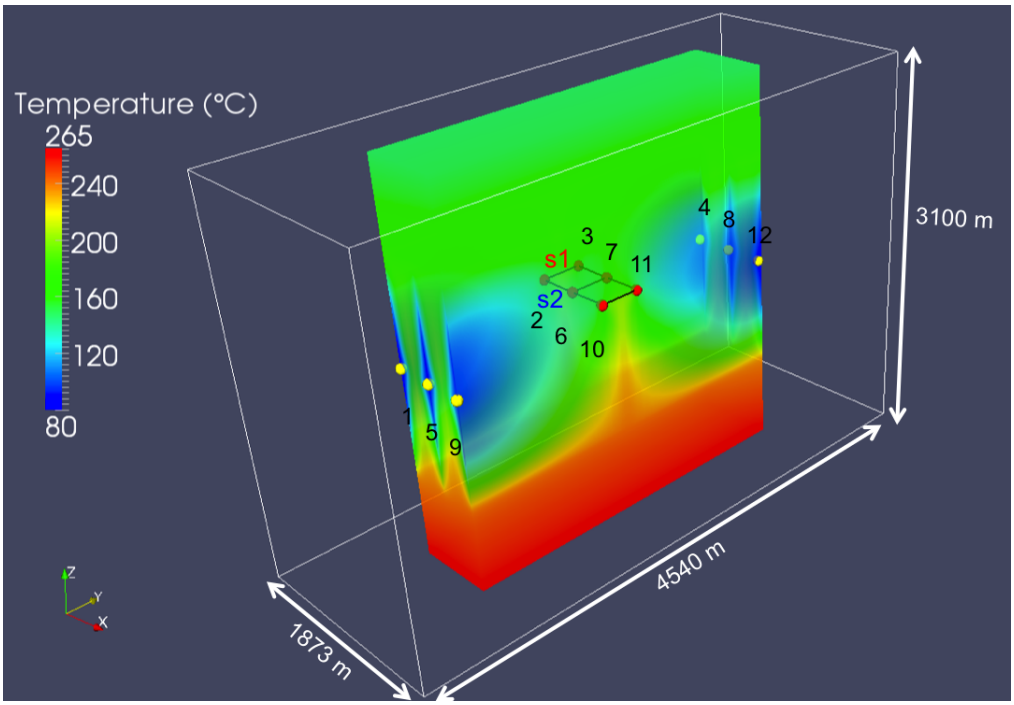

Figure 3.14: Subset of the reservoir volume along σ_1 highlighting the position of 6 doublets, with 4 wells in each fracture zone. Also shown are the separations *s1*, *s2* and six partial 'penny-shaped' heat-exchange areas. Yellow and red spheres represent the injectors and the producers respectively.

and peripheral (2, 3, 10 and 11) producers is around 5 °C implying interference between the wells. The overlapping of *heat-transfer volumes* is much higher in this case and it becomes detrimental to overall performance of the system.

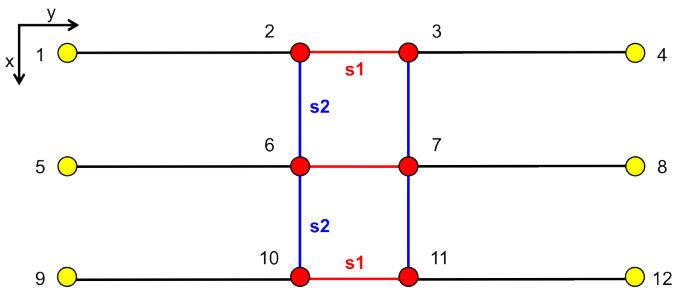

Figure 3.15: Plan view of the model with 6 doublets showing the position of 12 wells and the separations *s1* and *s2*. Note that the producers (red) are located 200 m higher than the injectors (yellow) (not to scale).

Similar results are obtained on reversing the doublets to have injectors in the middle. As shown in Fig. 3.16, this layout results in one big heat-exchange area instead of two smaller ones but it does not affect the performance of EGS. A separation of $s1 = s2 = 150\,\mathrm{m}$ has proven to be an optimal value when it comes to implementing multiple doublets in the same EGS reservoir irrespective of their polarities. See Appendix (Fig. A.1) for bottom-hole temperatures in this case. Both the layouts with 6 doublets correspond to an effective heat-exchange area of $8\,\mathrm{km}^2$ - $10\,\mathrm{km}^2$ and $2\,\mathrm{km}^3$ of accessible rock volume.

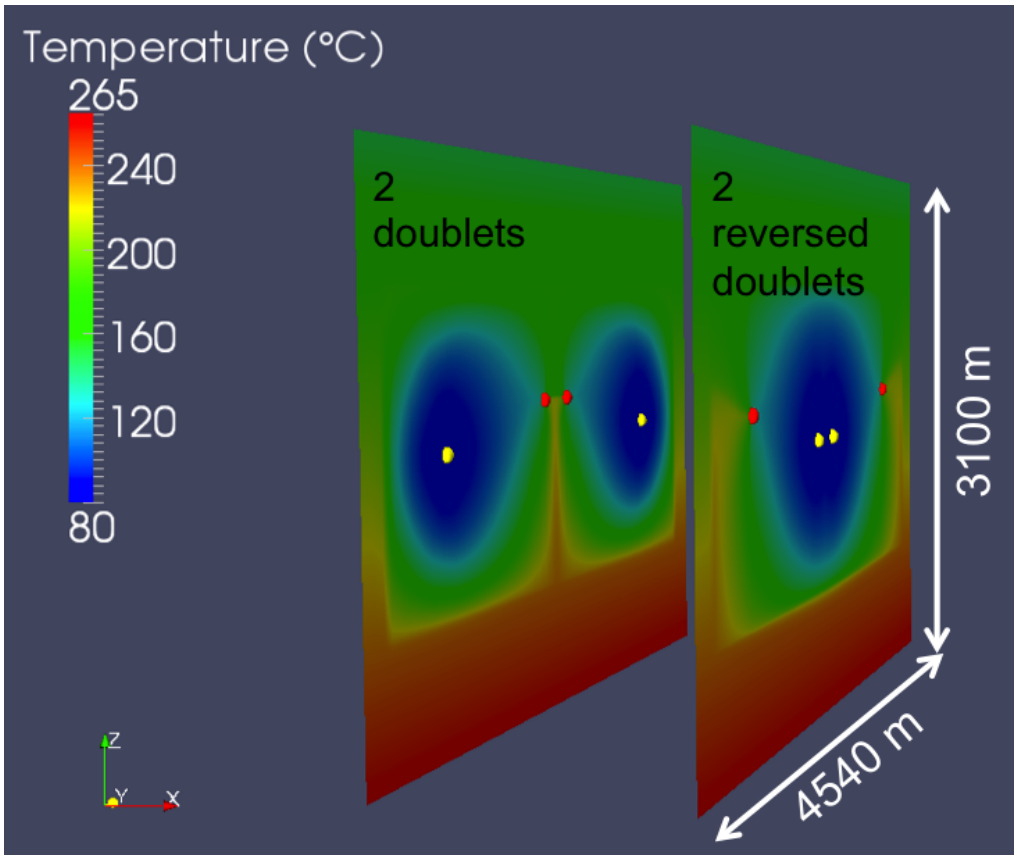

Figure 3.16: Cross sections along σ_1 depicting heat-exchange areas created by 2 doublets and 2 reversed doublets. Yellow and red spheres represent the injectors and the producers respectively.

3.6.2 Multiple Triplets

Building on the same model design as in 3.6.1, the new model is modified to have six triplets in 3 fracture zones (Zone5) enclosed within one surrounding zone (Zone4). There are 6 outer producers (1, 6, 7, 12, 13 and 18), 6 inner producers (3, 4, 9, 10, 15 and 16) and 6 injectors (2, 5, 8, 11, 14 and 17); totaling up to 18 wells with 6 in each fracture zone (Fig. 3.17 and 3.18). Again, separation *s1* represents the distance between producers of the same fracture zone and separation *s2* represents the distance between the producers of the adjacent fracture zones.

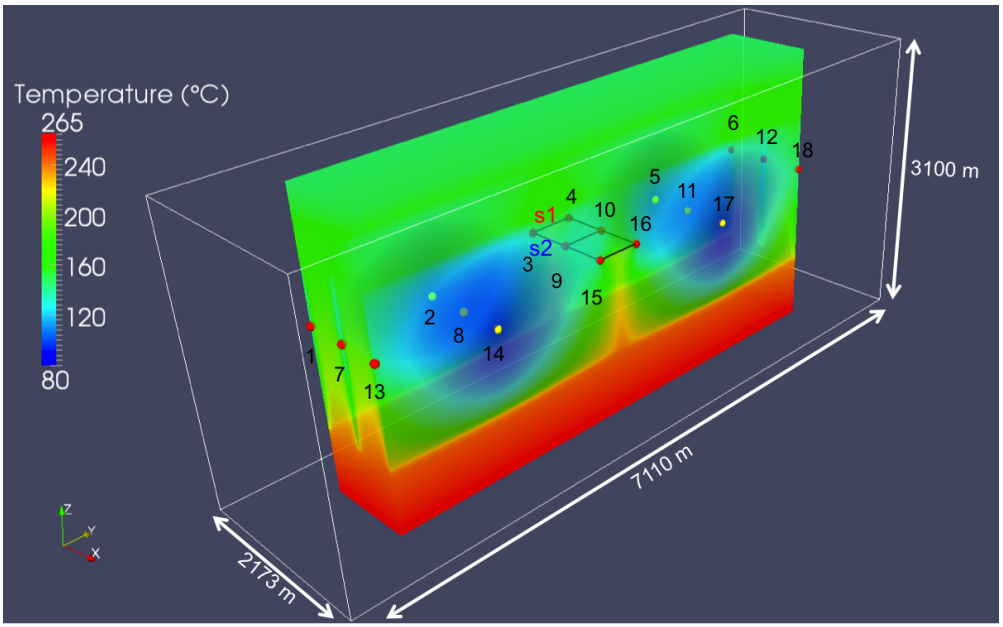

Figure 3.17: Subset of the reservoir volume along σ_1 highlighting the position of 6 triplets, with 6 wells in each fracture zone at an injection rate of $100\,\mathrm{L\,s^{-1}}$. Also shown are the separations *s1*, *s2* and the 'penny-shaped' heat-exchange areas. Yellow and red spheres represent the injectors and the producers respectively.

For a constant injection rate of $50\,\mathrm{L\,s^{-1}}$, five models are simulated where *s1* = *s2* = {150, 300, 450, 600, 750} m. For all separations, outer producers (1, 6, 7, 12, 13 and 18) give a thermal drawdown of 25 °C over 31 years and for inner producers (3, 4, 9, 10, 15 and 16), it varies between 26 °C - 30 °C. As seen in the case of doublets, the overlapping between *heat-transfer volumes* of adjacent fracture zones increases for smaller separations. A separation of *s1* = *s2* = 450 m is found to be optimal for installing multiple triplets.

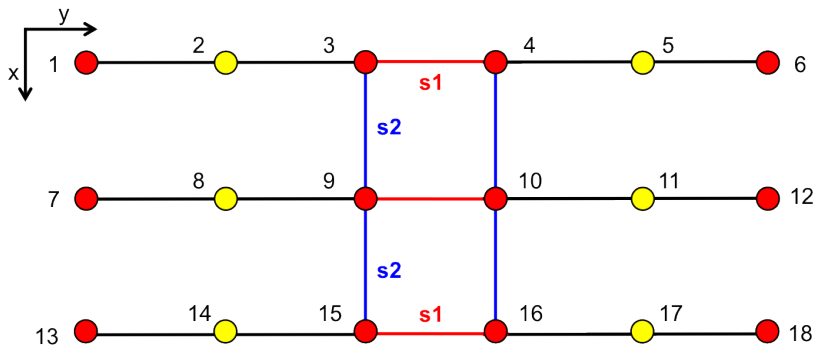

Figure 3.18: Plan view of the model with 6 triplets showing the position of 18 wells and the separations *s1* and *s2*. Note that producers (red) are located 200 m higher than the injectors (yellow) (not to scale).

It has been discussed in Section 3.5 that a triplet allows to inject geothermal fluids at higher flow rates without resulting in a short-circuit, thereby producing more energy over time. To take advantage of this, the EGS with multiple triplets is simulated with a higher flow rate of $100\,\mathrm{L\,s^{-1}}$. It is also shown in Section 3.4.2 that higher flow rates have bigger heat-transfer volumes, therefore the wells should not be placed very close to each other. Four models are created where *s1* = *s2* = {300, 450, 600, 750} m. After 31 years, the bottom-hole temperatures are around 150 °C for outer producers (1, 6, 7, 12, 13 and 18) and between 144 °C - 147 °C for inner producers (3, 4, 9, 10, 15 and 16) with lower temperatures at smaller separations. A balance has to be found between thermal drawdown and effectiveness of the combined heat-transfer volumes and a separation of *s1* = *s2* = 450 m serves the purpose very well. See Appendix (Fig. A.2) for bottom-hole temperatures in this case. This layout with 6 triplets corresponds to an effective heat-exchange area of $10\,\mathrm{km^2}$ - $12\,\mathrm{km^2}$ and $5\,\mathrm{km^3}$ of accessible rock volume. Here, the case of reversed triplets is not shown, as it creates a very high pressure drop in the reservoir with 6 wells injecting water at $100\,\mathrm{L\,s^{-1}}$ next to each other. To make sure that the injectors do not influence each other, they will have to be located at large distances from each other, thereby making the heat extraction inefficient.

Chapter 4

EGS Potential in Germany

Germany has witnessed a boom lately in terms of the installed capacity of geothermal heat pumps which are employed for space heating and hot water production. For the purpose of producing geothermal electricity and heat from deep reservoirs, 80 projects had been established by the end of the year 2006 [8], but only four projects at Unterhaching (3.4 MW_e) [6], Landau (3 MW_e) [5], Neustadt-Glewe (0.23 MW_e) [37] and Bruchsal (0.55 MW_e) [8, 30] are producing electricity as of today. Several EGS feasibility studies are underway in Germany but they all are still in their infancy. In the wake of the recent Fukushima Daiichi nuclear disaster in Japan; The Federal Government of Germany *(Die Bundesregierung Deutschland)* has decided to phase out nuclear power plants from the country by the year 2022. The reduced electricity production will have to be compensated by relying heavily on renewables.

[8] gives the gross power production in Germany for the year 2011 as 612 TW h. Renewables account for 20 % of it while the rest 80 % is being produced by nuclear power plants and combustion of fossil fuels. By the year 2050, Germany aims to produce bulk of its energy from renewable sources while cutting down greenhouse gas emissions in compliance with the Kyoto Protocol. Geothermal energy along with its versatile EGS systems can play a big role here but there is a need to estimate its overall potential. There have been some developments in the past which highlight the growing political and public interest in geothermal energy. The Renewable Energy Act (*Erneuerbare Energien Gesetz - EEG*) was ratified in the year 2000 [36]. It offers incentives to companies and industries linked with renewable energies in some capacity. EEG was amended in 2009 with increased EEG tariffs for geothermal power (Table 4.1) amid growing political support. The second highest EEG assistance per kW h is given to geothermal power production, next only to photovoltaics [16].

A comprehensive land-use based study has been done here to evaluate the EGS potential in Germany with a hope that such a potential calculation would help country's policy makers realize the potential contribution of EGS systems towards future energy market. And that they would grant more incentives to

industry partners who venture into geothermal electricity production.

Table 4.1: EEG 2009 feed-in tariffs for geothermal power (adapted from [16]).

Scenario	**Capacity** $\leq$ **10 MW**$_e$	**Capacity** $>$ **10 MW**$_e$
EEG base tariff [€per kW h]	0.16	0.105
Start of operation before 2016	0.04	0.04
Cogeneration of heat and power	0.03	0.03
Utilization of EGS techniques	0.04	0.04
Maximum tariff obtainable	0.27	0.215

4.1 Available Land Area

Germany has a land area of 348,672 km^2 [13] with another 8350 km^2 covered by water. Jung et al. [24] propose three potential crystalline areas around Germany for geothermal power generation in the depth range of 3 km - 7 km using HDR technology (Fig. 4.1). Unlike HDR, EGS is independent of the availability of hot water from the reservoir and hence all three HDR potential areas are also considered as a potential source for electricity production using EGS technologies. These sources are the Central and Southern German crystalline area, the Upper Rhine Valley crystalline area and the Rotliegend volcanics occurring in the North-German basin where average geothermal gradient is around 30 °C km^{-1}. All these areas correspond to a minimum temperature of 100 °C - 130 °C at a depth of 3 km. A temperature of 150 °C has been defined at a depth of 4 km in the SHEMAT models, so the models are in agreement with the actual temperature values.

The crystalline area map (Fig. 4.1) is considered as a base for the potential calculation. Using the longitudinal and latitudinal distances [31], the land area of Germany is determined as 350,592 km^2 from the map. A marginal 0.5 % increase from the actual land area is observed here thus highlighting the high accuracy and reliability of the calculation. Next, area covered by the crystalline rocks acting as the potential source is worked out. Only a portion of this crystalline area can be used for engineering EGS reservoirs owing to competing land uses. A lot of land comes under protected areas which are designated for sustainable development and have restrictions on land use. Nature parks, biosphere reserves and national parks are three different types of protected areas which can be overlapping or not depending on the region. BfN [4] defines the main purpose of these areas as to protect and conserve the natural landscape by providing a safe haven for its diverse species and habitats. Hence, the area covered by

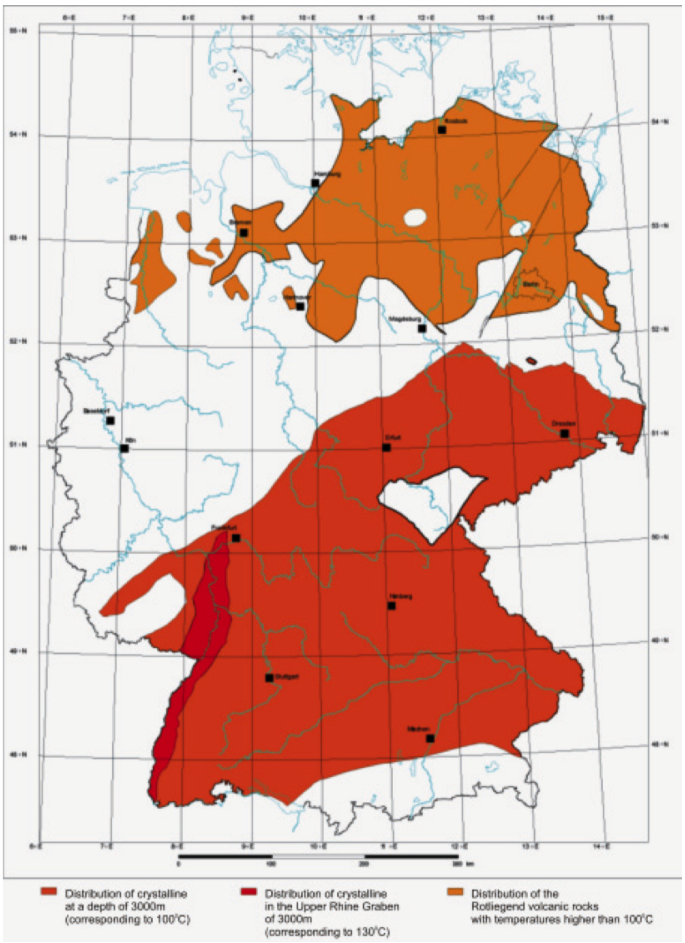

Figure 4.1: Map depicting the occurrence of crystalline rocks in Germany which are considered as a potential area for electricity production using EGS technologies. Rotliegend volcanics are shown in orange while the Central and Southern German crystalline area is shown in red [24].

protected areas in the crystalline regions is excluded from the potential study by comparing the available maps and datasets. See Appendix (Fig. A.4, A.5 and A.6) for maps of biosphere reserves, national parks and nature parks in Germany. Also given is the list of protected areas that have been excluded from the potential calculations (Table B.2 and B.3).

As the EGS reservoirs are prone to induced seismicity because of fluid injections in the subsurface (Section 2.2), seismically hazardous regions also need to be removed from the potential calculations. Seismically active regions are primarily located around Rhine Rift Valley and Leipzig. An initiative by GFZ Potsdam has produced a seismic hazard map for Germany, Austria and Switzerland [22]. On the basis of Instrumental Intensities [40], the map outlines zones

with different scales of potential damage that could happen in that zone in case of an earthquake (see Appendix, Fig. A.3). Zones with intensities VI (corresponding to light potential damage) and above are excluded from the remaining crystalline area (see Appendix, Table B.1). Furthermore, another 6.7 % and 4.9 % of the leftover area are subtracted accounting for infrastructure and traffic respectively [7], leaving behind the crystalline area with an EGS potential as 89000 km^2 (Fig. 4.2). It is around one-fourth of Germany's land area or 44 % of the actual crystalline area. The well field area varies between 5 km^2 - 15 km^2 for EGS systems. Theoretically, there is enough potential crystalline area to support 11860 EGS systems with 6 doublets (for an average area of 7.5 km^2), or 7120 EGS systems with 6 triplets (for an average area of 12.5 km^2). How that translates into terms of produced energy and electrical power is discussed in the next section.

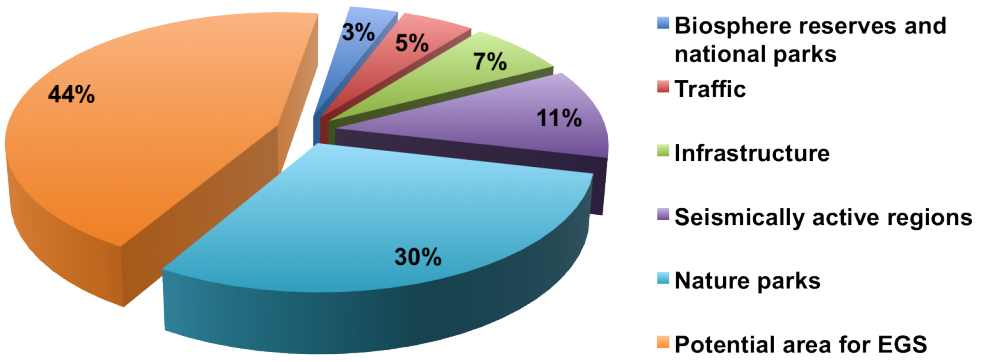

Figure 4.2: Competing land use types in the crystalline area of Germany. Area with EGS potential is around 89000 km^2.

4.2 Energy and Power

Thermal power from the production wells over time is evaluated using the relation:

$$P_t = \rho_f \cdot c_p \cdot \Delta T \cdot Q \tag{4.1}$$

where P_t is the thermal power (W), ρ_f is the fluid density ($\mathrm{kg\,m^{-3}}$), c_p is the specific heat capacity ($\mathrm{J\,kg^{-1}\,K^{-1}}$), ΔT = T - 80; is the temperature difference (°C) and Q is the volumetric production flow rate ($\mathrm{m^3\,s^{-1}}$). At 200 °C, water density is taken as $862\,\mathrm{kg\,m^{-3}}$ and a value of $4510\,\mathrm{J\,kg^{-1}\,K^{-1}}$ is used for the specific heat capacity of water. It is assumed that there is no temperature drop while the geothermal fluids are ascending through the cooler sections of the crust. As the borehole heats up with time, the temperature drop decreases.

Considering a binary plant at the surface working on ORC with a net efficiency of 10 % (11.4 % at Soultz-sous-Forêts [21]), and accounting for the installation consumption by the pumps, electrical power is given as:

$$P_e = (P_t \cdot \varepsilon) - ic \tag{4.2}$$

where P_e is the electrical power (W), ε is the net efficiency of Organic Rankine Cycle (ORC) and ic is the installation consumption.

A 4^{th} degree polynomial fit is obtained for the thermal power curve, and it is integrated over time to give the total thermal energy produced. Electrical energy is evaluated in the same way. Thermal and electrical power for EGS systems with 6 triplets or 6 doublets are compared in Fig. 4.3.

To estimate the potential power, we first look at the heat available in 1 km thick basement at a depth of 5 km below the potential area of $89000\,\mathrm{km^2}$ (calculated in Section 4.1):

$$H = \rho_r \cdot c_p \cdot V \cdot (T_x - T_r) \tag{4.3}$$

where H is the heat energy (J), ρ_r is the density of granite ($\mathrm{kg\,m^{-3}}$), c_p is the specific heat capacity of granite ($\mathrm{J\,kg^{-1}\,K^{-1}}$), V is the volume ($\mathrm{m^3}$), T_x is the average temperature of the volume of crust (°C) and T_r is the temperature to which the crust can be reduced (°C) [2]. Using the values $\rho_r = 2710\,\mathrm{kg\,m^{-3}}$, $c_p = 790\,\mathrm{J\,kg^{-1}\,K^{-1}}$, $V = 89000\,\mathrm{km^3}$, $T_x = 200\,°\mathrm{C}$ and $T_r = 160\,°\mathrm{C}$, we get available heat H as 7621 EJ.

For a plant's operation life span of 31 years, potential electric power is then given as:

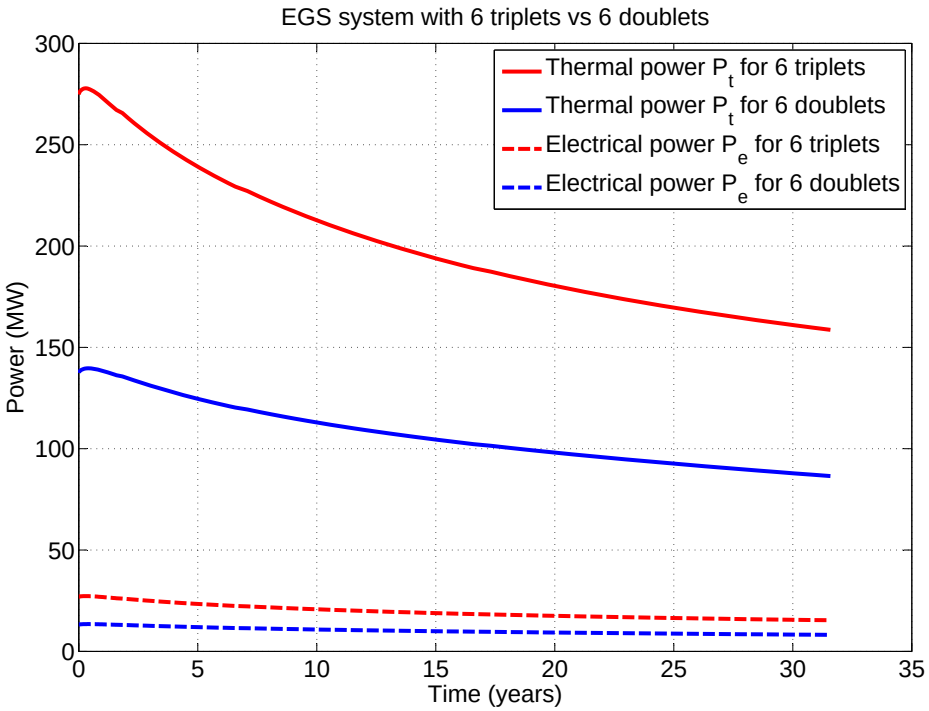

Figure 4.3: Comparison of thermal and electric power given by different EGS layouts. Average electric power of 6 triplets (injection flow rate of $100\,\mathrm{L\,s^{-1}}$) and 6 doublets (injection flow rate of $50\,\mathrm{L\,s^{-1}}$) are $20\,\mathrm{MW}_e$ and $10\,\mathrm{MW}_e$ respectively.

$$P = (H \cdot \varepsilon)/(31 \cdot 365 \cdot 86400) \tag{4.4}$$

For an efficiency $\varepsilon = 0.1$, potential electric power is evaluated as $780\,\mathrm{GW}_e$. This potential calculation lies somewhere between *theoretical* and *technical* potentials. Beardsmore [2] define *theoretical* potential as the physically usable energy supply over a certain time span in a given region, while *technical* potential is only a fraction of it that can be used owing to technical or structural restrictions. Areas which limit the possibility of EGS have been excluded already in these calculations, hence the calculated potential is smaller than the *theoretical* potential. Since, parameters like *maximum allowable temperature drawdown* and *recoverability factor* given by [2] are not considered here, this potential calculation is slightly higher than the *technical* potential.

Taking an average area of $12.5\,\mathrm{km}^2$ for a EGS system with 6 triplets, the number of installations possible in the country is 7120. With an average electric power of $20\,\mathrm{MW}_e$, these installations would collectively yield an extractable potential power of $142\,\mathrm{GW}_e$. This is around 18 % of total potential ($780\,\mathrm{GW}_e$) calculated on the basis of available heat in the subsurface. Considering an operation time of 31 years and covering a resource base for 200 years, we get an

installed capacity of 22.01 GW_e at any time. Assuming that these 7120 plants are running all year-round, this corresponds to 192 TW h of electric energy produced in a year which is around 30 % of Germany's gross power production in 2011. Table 4.2 compares the potential of different EGS layouts.

Table 4.2: Potential of different EGS layouts.

Parameter	**6 triplets**	**6 doublets**
Thermal energy in 31 years (EJ)	0.20	0.10
Average thermal power (MW_t)	200	100
Average electric power (MW_e)	20	10
Electrical energy in 1 year (TW h)	0.17	0.087
Systems possible in 89000 km^2	7120	11860
Extractable potential power (GW_e)	142	119
Systems for 20 % of 612 TW h	720	1400
Area required (km^2)	9000	10500
Available heat (EJ)	7621	7621
Overall potential (GW_e)	780	780

Chapter 5

Conclusion

Engineered Geothermal Systems have the capacity to exploit the thermal heat stored within the Earth's crust irrespective of the reservoir rock permeability or availability of geothermal fluids. After reviewing the available literature and considering the valuable lessons learnt from previous EGS studies around the world, this work identifies core issues which hinder an EGS project's success. Production flow rates and well separation are two such parameters which govern EGS reservoir's transmissivity and ultimately the EGS system's performance. Forward modelling code SHEMAT has been used to establish large-scale response of reservoir rock towards fluid injections. By varying the parameters systematically, the task of optimizing the system has been accomplished here and two different EGS layouts are proposed for achieving efficient heat mining from the reservoirs. Both layouts consist of 3 vertical fracture zones engineered next to each other in the subsurface at different separations. The first layout is composed of 6 doublets (or 6 reversed doublets) with 4 wells in each fracture zone which are located at a separation of 150 m. Operating the system at a production flow rate of $50\,\mathrm{L\,s^{-1}}$ for 31 years yields an average electric power of $10\,\mathrm{MW}_e$. The second layout comprises 6 triplets with 18 wells drilled in three fracture zones which are separated by 450 m. For an operation time of 31 years, this EGS system supplies $20\,\mathrm{MW}_e$ of average electric power at a constant fluid injection rate of $100\,\mathrm{L\,s^{-1}}$. Although the simulations have been carried out for 3 vertical fracture zones, the layouts can be extrapolated easily for a desired number of fracture zones.

Furthermore, the potential area for EGS systems has been evaluated for Germany by a comprehensive study of available land area and competing land uses. Basing the calculation on the crystalline regions in the country and excluding the land area covered by protected areas, seismically hazardous zones, infrastructure and traffic, an area of $89000\,\mathrm{km}^2$ is identified for EGS potential. Potential power that can be extracted by EGS systems from this area has been computed and compared to overall potential. EGS systems provide non-intermittent power, have a minor surface footprint and cause low to zero carbon emissions. To conclude, renewables like geothermal energy including its EGS systems will play a vital role in building a greener tomorrow.

Bibliography

[1] Baria, R., Baumgärtner, J., Gérard, A., Jung, R., and Garnish, J. European HDR research programme at Soultz-sous-Forêts (France) 1987-1996. *Geothermics 28*, 4-5 (1999), 655–669.

[2] Beardsmore, G. R., Rybach, L., Blackwell, D., and Baron, C. A Protocol for Estimating and Mapping Global EGS Potential. In *Proceedings, Geothermal Resources Council Annual Meeting 2010* (2011), International Energy Agency, Paris Cedex. `http://bit.ly/Vni9SL`, retrieved: 06.12.2012.

[3] Bertani, R. Long term projection of geothermal electricity development in the world. In *Proceedings, GeoTHERM conference, Offenburg* (2009). `http://bit.ly/LAYhvS`, retrieved: 06.12.2012.

[4] BfN. Protected Areas. Bundesamt für Naturschutz (BfN), Bonn, 2011. `http://bit.ly/N7uoQt`, retrieved: 06.12.2012.

[5] BINE. Geothermische Stromerzeugung in Landau. Bundesministerium für Wirtschaft und Technologie, Berlin, 2007. `http://bit.ly/YByOJW`, retrieved: 06.12.2012.

[6] BINE. Geothermal electricity generation combined with a heating network. Bundesministerium für Wirtschaft und Technologie, Berlin, 2009. `http://bit.ly/TKlo7s`, retrieved: 06.12.2012.

[7] BMELV. Farming in Germany. Bundesministerium für Ernährung, Landwirtschaft und Verbraucherschutz (BMELV), Bonn, 2004. `http://bit.ly/Nxi4ON`, retrieved: 06.12.2012.

[8] BMWi. Research for an environmentally sound, reliable and affordable energy supply - 6^{th} Energy Research Programme of the Federal Government. Bundesministerium für Wirtschaft und Technologie (BMWi), Berlin, 2012. `http://bit.ly/XrCJHM`, retrieved: 06.12.2012.

[9] Boussinesq, J. *Théorie analytique de la chaleur*. Gauthier-Villars, Paris, 1903.

[10] Breesee, J. C., Ed. *The Soultz Hot Dry Rock Project*. Gordon and Breach, Philadelphia, 1992.

[11] BROWN, D., DUTEAUX, R., KRUGER, P., SWANSON, D., AND YAMAGUCHI, T. Fluid circulation and heat extraction from engineered geothermal reservoirs. *Geothermics 28*, 4-5 (1999), 553–572.

[12] BROWN, D. W., AND DUCHANE, D. V. Scientific progress on the Fenton Hill HDR project since 1983. *Geothermics 28*, 4-5 (1999), 591–601.

[13] CIA. World Factbook - Germany. Central Intelligence Agency (CIA), Washington D.C., 2012. `http://1.usa.gov/3M2asP`, retrieved: 06.12.2012.

[14] CLAUSER, C., Ed. *Numerical Simulation of Reactive Flow in Hot Aquifers: SHEMAT and Processing SHEMAT*. Springer, Heidelberg-Berlin, 2003.

[15] CLAUSER, C. Geothermal Energy. In *Landolt-Börnstein, Group VIII: Advanced Material and Technologies, Vol. 3: Energy Technologies, Subvol. C: Renewable Energies*, K. Heinloth, Ed. Springer, Heidelberg-Berlin, 2006, pp. 493–604.

[16] DEUTSCHERBUNDESTAG. Gesetz zur Neuregelung des Rechts der Erneuerbaren Energien im Strombereich und zur Änderung damit zusammenhängender Vorschriften vom 25 Oktober 2008. *Bundesgesetzblatt 2008*, 49 (2008), 2074–2100.

[17] DUFFIELD, W. A., AND SASS, J. H. *Geothermal Energy - Clean Power From the Earth's Heat*. U.S. Geological Survey, Reston, 2003. `http://on.doi.gov/15Jo8Q`, retrieved: 06.12.2012.

[18] ECONOMIDES, M. J., AND NOLTE, K. G., Eds. *Reservoir Stimulation, 3rd ed.* John Wiley, Hoboken, New Jersey, 2003.

[19] FREEZE, A. R., AND CHERRY, J. A. *Groundwater*. Prentice Hall, New Jersey, 1979.

[20] GALLUP, D. L. Production engineering in geothermal technology: A review. *Geothermics 38*, 3 (2009), 326–334.

[21] GENTER, A., FRITSCH, D., CUENOT, N., BAUMGÄRTNER, J., AND GRAFF, J. J. Overview of the Current Activities of the European EGS Soultz Project: from Exploration to Electricity Production. In *Proceedings, Thirty-Fourth Workshop on Geothermal Reservoir Engineering, 9-11 February 2009* (2009), Stanford University, California. `http://bit.ly/VEFBNn`, retrieved: 06.12.2012.

[22] GRÜNTHAL, G. Erdbeben und Erdbebengefährdung in Deutschland sowie im Europäischen Kontext. *Geographie und Schule 151*, 26 (2004), 14–23.

[23] HEIDINGER, P. Integral modeling and financial impact of the geothermal situation and power plant at Soultz-sous-Forêts. *Comptes Rendus Geoscience 342*, 7-8 (2010), 626–635.

[24] Jung, R., Röhling, S., Ochmann, N., Rogge, S., Schellschmidt, R., Schulz, R., and Thielemann, T. *Abschätzung des technischen Potenzials der geothermischen Stromerzeugung und der geothermischen Kraft-wärmekopplung (KWK) in Deutschland - Bericht für das Büro für Technikfolgenabschätzung beim Deutschen Bundestag.* Institut für Geowissenschaftliche Gemeinschaftsaufgaben, Hannover, Bundesanstalt für Geowissenschaften and Rohstoffe, Hannover, Institut für Energiewirtschaft und Rationelle Energieanwendung, Universität Stuttgart, 2002.

[25] Kolditz, O., and Clauser, C. Numerical simulation of flow and heat transfer in fractured crystalline rocks: Application to the Hot Dry Rock site in Rosemanowes (U.K.). *Geothermics 27*, 1 (1998), 1–23.

[26] Kühn, M., Bartels, J., and Iffland, J. Predicting reservoir property trends under heat exploitation: interaction between flow, heat transfer, transport, and chemical reactions in a deep aquifer at Stralsund, Germany. *Geothermics 31*, 6 (2002), 725–749.

[27] Majer, Ernest L and Baria, Roy and Stark, Mitch and Oates, Stephen and Bommer, Julian and Smith, Bill and Asanuma, Hiroshi. Induced seismicity associated with Enhanced Geothermal Systems. *Geothermics 36*, 3 (2007), 185–222.

[28] McDonald, Robert I. and Fargione, Joseph and Kiesecker, Joe and Miller, William M. and Powell, Jimmie. Energy Sprawl or Energy Efficiency: Climate Policy Impacts on Natural Habitat for the United States of America. *PLoS ONE 4*, 8 (2009), e6802.

[29] McKelvey, V. E. Mineral Resource Estimates and Public Policy. *American Scientist 60*, 1 (1972), 32–40.

[30] Münch, W., Kölbel, T., Herzberger, P., Schlagermann, P., Hötzl, H., Wolf, L., Rettenmaier, D., Steger, H., Zorn, R., Seib, P., Möllmann, G., Sauter, M., Ghergut, J., and Ptak, T. The Geothermal Power Plant Bruchsal. In *Proceedings, World Geothermal Congress 2010 Bali, Indonesia, 25-29 April 2010* (2010).

[31] NCEDC. Distance Conversion. National California Earthquake Data Center (NCEDC), Berkeley, California, 2012. `http://bit.ly/SOboea`, retrieved: 06.12.2012.

[32] NOAA. Water Density Calculator. National Oceanic Atmospheric Administration (NOAA), Washington D.C. and Michigan State University, Michigan, 2012. `http://bit.ly/fQzVL`, retrieved 06.12.2012.

[33] Oberbeck, A. Ueber die Wärmeleitung der Flüssigkeiten bei Berücksichtigung der Strömungen infolge von Temperaturdifferenzen. *Annalen der Physik 243*, 6 (1879), 271–292.

[34] Parker, R. The Rosemanowes HDR project 1983-1991. *Geothermics 28*, 4-5 (1999), 603–615.

[35] Pettitt, W., Pierce, M., Damjanac, B., Hazzard, J., Lorig, L., Fairhurst, C., Gil, I., Sanchez, M., Nagel, N., Reyes-Montes, J., and Young, R. P. Fracture network engineering for hydraulic fracturing. *The Leading Edge 30*, 8 (2011), 844–853.

[36] Purkus, A., and Barth, V. Geothermal power production in future electricity markets - A scenario analysis for Germany. *Energy Policy 39*, 1 (2011), 349–357.

[37] Schellschmidt, R., Sanner, B., Pester, S., and Schulz, R. Geothermal Energy Use in Germany. In *Proceedings, World Geothermal Congress 2010 Bali, Indonesia, 25-29 April 2010* (2010). `http://bit.ly/11W24cj`, retrieved: 06.12.2012.

[38] SLB. Hydraulic fracturing. Schlumberger Limited, Houston, 2012. http://bit.ly/OEhUmz, retrieved 23.07.2012.

[39] Tester, J. W., Anderson, B. J., Batchelor, A. S., Blackwell, D. D., DiPippo, R., Drake, E. M., Garnish, J., Livesay, B., Moore, M. C., Nichols, K., Petty, S., Nafi Toksoz, M., Veatch, R. W., Baria, R., Augustine, C., Murphy, E., Negraru, P., and Richards, M. *The Future of Geothermal Energy - Impact of enhanced geothermal systems on the United States energy supply in the 21st century.* Massachusetts Institute of Technology, Cambridge, 2006.

[40] USGS. ShakeMap Scientific Background. United States Geological Survey, Reston, 2011. http://earthquake.usgs.gov/earthquakes/shakemap/background.php, retrieved: 23.07.2012.

[41] Vogt, C., Kosack, C., and Marquart, G. Stochastic inversion of the tracer experiment of the enhanced geothermal system demonstration reservoir in Soultz-sous-Forêts - Revealing pathways and estimating permeability distribution. *Geothermics 42*, 0 (2012), 1–12.

[42] Zimmermann, G., Moeck, I., and Blöcher, G. Cyclic waterfrac stimulation to develop an Enhanced Geothermal System (EGS)-Conceptual design and experimental results. *Geothermics 39*, 1 (2010), 59–69.

Appendix A

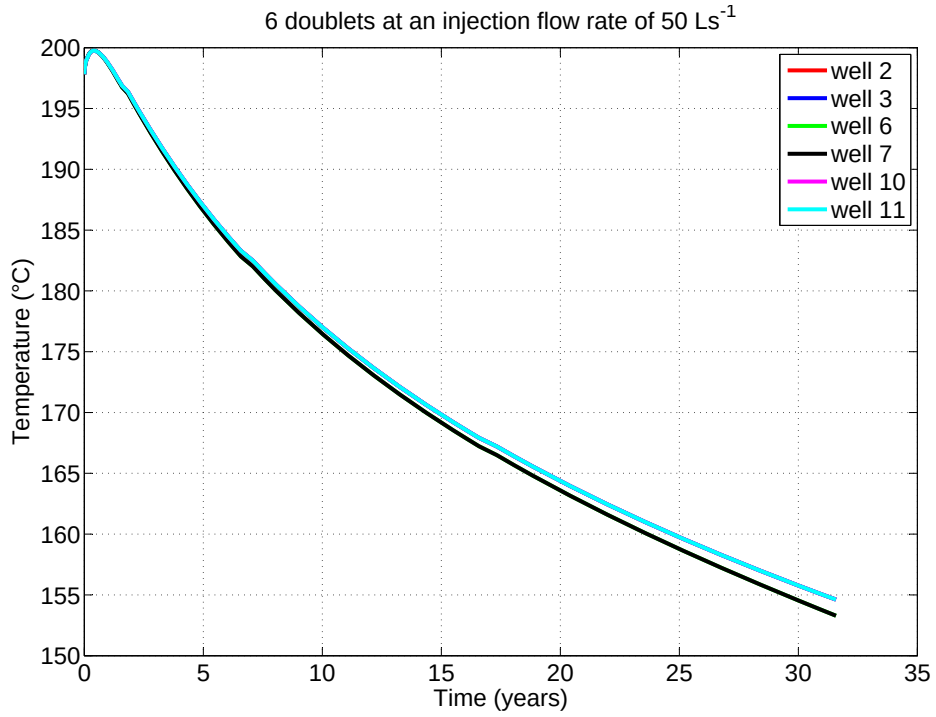

Figure A.1: Bottom-hole temperatures for 6 producers in an EGS layout with 6 doublets at separation $s1 = s2 = 150\,\mathrm{m}$. Thermal drawdown for the central producers (6 and 7) is $1\,^{\circ}\mathrm{C}$ higher than for the peripheral producers (2, 3, 10 and 11).

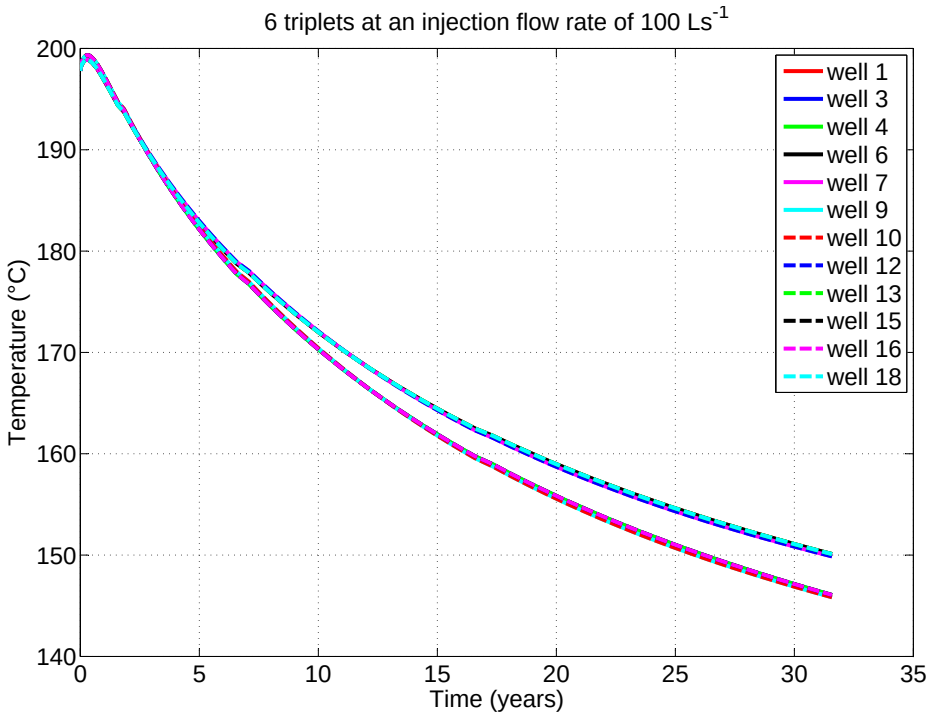

Figure A.2: Bottom-hole temperatures for 12 producers in an EGS layout with 6 triplets at separation $s1 = s2 = 450\,\mathrm{m}$. Thermal drawdown for the inner producers (3, 4, 9, 10, 15 and 16) is 4 °C higher than for the outer producers (1, 6, 7, 12, 13 and 18).

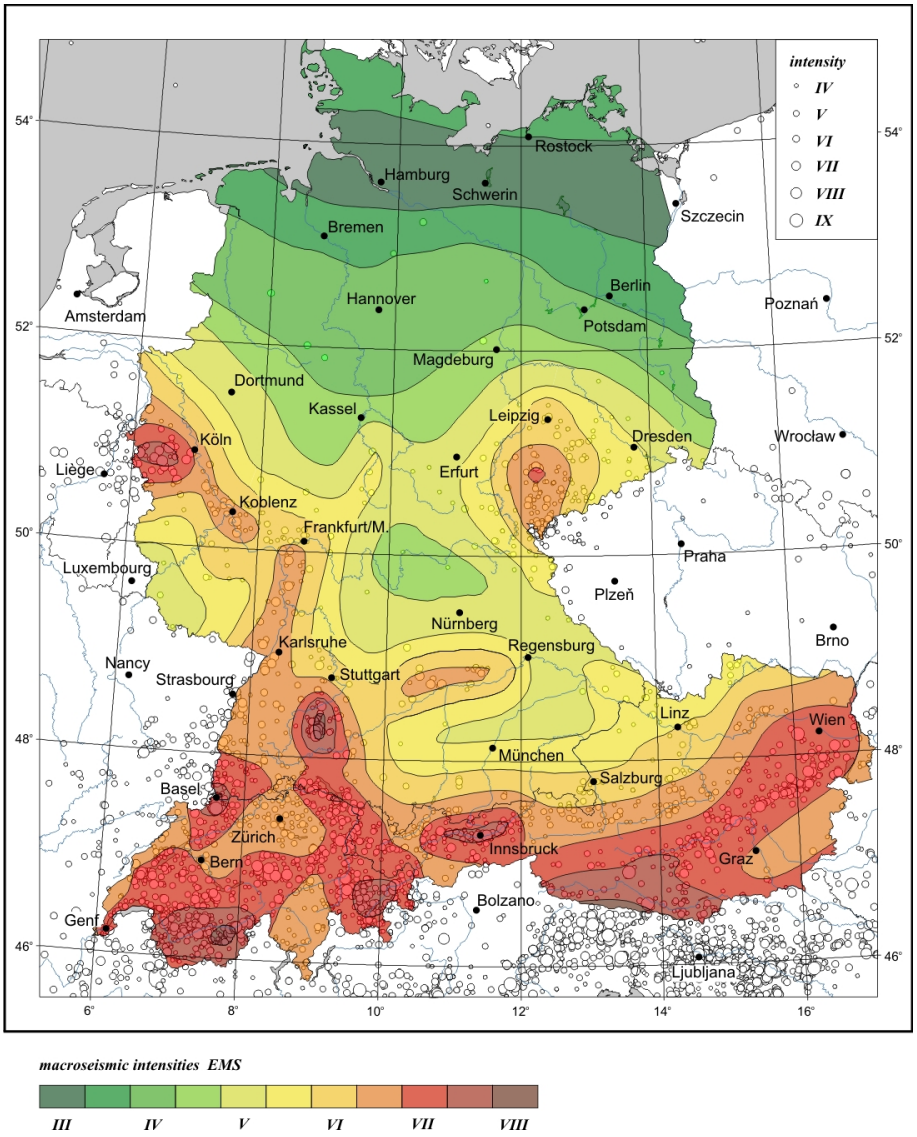

Figure A.3: Seismic hazard map for Germany, Austria and Switzerland showing zones with different Instrumental Intensities [22].

Figure A.4: Biosphere reserves in Germany [4].

Figure A.5: National parks in Germany [4].

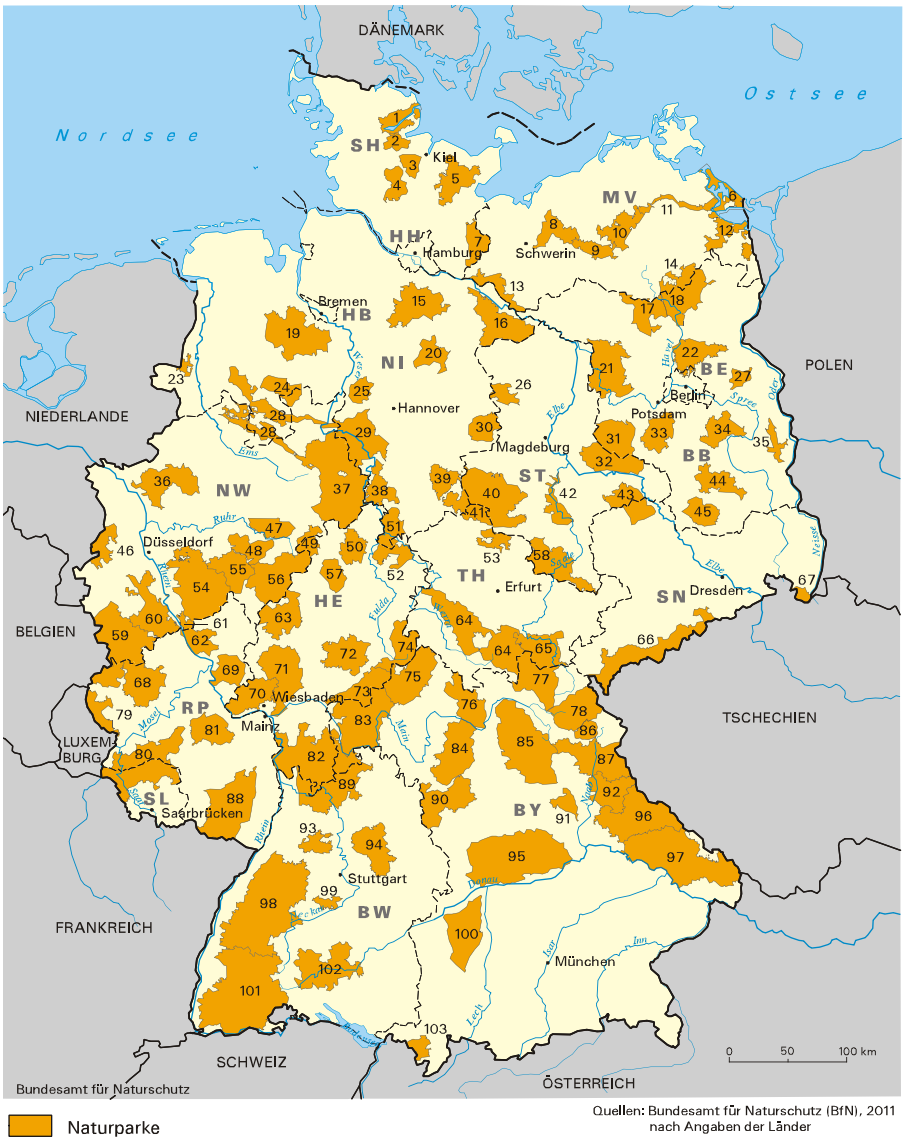

Figure A.6: Nature parks in Germany [4].

Appendix B

Appendix B

Table B.1: Description of Instrumental Intensities (adapted from [40]).

Instrumental Intensity	**Peak vel. (cms^{-1})**	**Peak acc. (%g)**	**Potential damage**	**Perceived shaking**
I	< 0.1	< 0.17	none	not felt
II-III	0.1 - 1.1	0.17 - 1.4	none	weak
IV	1.1 - 3.4	1.4 - 3.9	none	light
V	3.4 - 8.1	3.9 - 9.2	very light	moderate
VI	8.1 - 16	9.2 - 18	light	strong
VII	16 - 31	18 - 34	moderate	very strong
VIII	31 - 60	34 - 65	moderate/heavy	severe
IX	60 - 116	65 - 124	heavy	violent
X+	> 116	> 124	very heavy	extreme

Table B.2: A - List of protected areas considered for exclusion from the EGS potential calculation. Note that for some entities, only a fraction of their area is excluded depending on their overlapping with the crystalline area [4].

Name (State)	**Area (km^2)**	**Code**
Biosphere reserves		
Schaalsee (MV)	309	-
Schorfheide-Chorin (BB)	1292	-
Flusslandschaft Elbe (BB, MV, NI, SH, ST)	2759	-
Spreewald (BB)	475	-
Oberlausitzer Heide-und Teichlandschaft (SN)	301	-
Vessertal-Thüringer Wald (TH)	171	-
Schwäbische Alb (BW)	853	-
National parks		
Sächsische Schweiz (SN)	94	-
Müritz-Nationalpark (MV)	322	-
Unteres Odertal (BB)	103	-
Nature parks		
Holsteinische Schweiz (SH)	759	5
Lauenburgische Seen (SH)	474	7
Sternberger Seenland (MV)	540	8
Nossentiner/Schwinzer Heide (MV)	365	9
Mecklenburgische Schweiz und Kummerower See (MV)	616	10
Flusslandschaft Peenetal (MV)	334	11
Am Stettiner Haff (MV)	572	12
Mecklenburgisches Elbetal (MV)	426	13
Feldberger Seenlandschaft (MV)	360	14
Lüneburger Heide (NI)	1078	15
Elbhöhen-Wendland (NI)	1160	16
Stechlin-Ruppiner Land (BB)	680	17
Westhavelland (BB)	1294	21
Barnim (BB/BE)	733	22
Unteres Saaletal (ST)	408	42
Dübener Heide (SN/ST)	760	43
Niederlausitzer Heidelandschaft (BB)	490	45
Meißner-Kaufunger-Wald (HE)	422	52
Kyffhäuser (TH)	305	53
Saale-Unstrut-Triasland (ST)	1037	58
Thüringer Wald (TH)	2082	64

Table B.3: B - List of protected areas considered for exclusion from the EGS potential calculation. Note that for some entities, only a fraction of their area is excluded depending on their overlapping with the crystalline area [4].

Name (State)	**Area (km^2)**	**Code**
Nature parks		
Erzgebirge/Vogtland (SN)	1495	66
Zittauer Gebirge (SN)	133	67
Rhein-Taunus (HE)	804	70
Hochtaunus (HE)	1322	71
Hoher Vogelsberg (HE)	883	72
Hessischer Spessart (HE)	736	73
Hessische Rhön (HE)	723	73
Bayerische Rhön (BY)	1236	75
Haßberge (BY)	817	76
Fichtelgebirge (BY)	1011	78
Saar-Hunsrück (SL/RP)	1956	80
Soonwald-Nahe (RP)	736	81
Bergstraße-Odenwald (HE/BY)	2238	82
Bayerischer Spessart (BY)	1702	83
Steigerwald (BY)	1269	84
Fränkische Schweiz-Veldensteiner Forst (BY)	2335	85
Steinwald (BY)	230	86
Nördlicher Oberpfälzer Wald (BY)	1287	87
Pfälzerwald (RP)	1793	88
Neckartal-Odenwald (BW)	1292	89
Frankenhöhe (BY)	1104	90
Hirschwald (BY)	278	91
Oberpfälzer Wald (BY)	823	92
Stromberg-Heuchelberg (BW)	329	93
Schwäbisch-Fränkischer Wald (BW)	904	94
Altmühltal (BY)	2966	95
Oberer Bayerischer Wald (BY)	1733	96
Bayerischer Wald (BY)	2783	97
Schwarzwald Mitte/Nord (BW)	3740	98
Schönbuch (BW)	156	99
Augsburg-Westliche Wälder (BY)	1225	100
Südschwarzwald (BW)	3700	101
Obere Donau (BW)	1350	102